Usher syndrome Type 1-associated gene, *pcdh15b*, is required for photoreceptor structural integrity in zebrafish

Amanda Miles[1], Clarke Blair[1], Andrew Emili[2] & Vincent Tropepe[1,*]

[1]Department of Cell and Systems Biology, University of Toronto, Toronto, Canada
[2]Center for Network Systems Biology, Boston University, Boston, MA, USA

***Corresponding author:** Vincent Tropepe
v.tropepe@utoronto.ca
25 Harbord St.
University of Toronto
Toronto, ON, M5S 3G5

Conflict of interest
The authors declare no competing financial interests.

Acknowledgments
We thank the CSB imaging staff including Audrey Chong for TEM/SEM assistance, and Henry Hong for confocal microscopy assistance. Cacna1fa antibody was kindly provided by Dr. Michael Taylor. We would also like to thank all members of the Tropepe lab, Debanjan Barua and Ashley Miles for comments on the manuscript. This work is supported by a Fighting Blindness Canada Grant to VT. AM is supported by a doctoral scholarship from the Natural Sciences and Engineering Research Council of Canada (NSERC-CGS-D).

Contributions
AM, AE and VT designed the research. AM performed all the experiments, with assistance from CB for TEM and immunostaining experiments. AM and VT analyzed the data. AM wrote the manuscript. VT supervised the project.

Abstract

Blindness associated with Usher Syndrome Type 1 (USH1) is typically characterized as rod photoreceptor degeneration, followed by secondary loss of cones. The mechanisms leading to blindness are unknown since most genetic mouse models only recapitulate auditory defects. We generated zebrafish mutants for one of the USH1 proteins, *protocadherin-15b* (*pcdh15b*), a putative cell adhesion molecule. Zebrafish *pcdh15* is expressed exclusively in photoreceptors

within calyceal processes (CPs), at the base of the outer segment (OS), and within the synapse. In our mutants, rod and cone photoreceptor integrity is compromised with early and progressively worsening abnormal OS disc growth and detachment, in part due to weakening CP contacts. These effects were attenuated or exacerbated by growth in dark and bright light conditions, respectively. We also describe novel evidence for structural defects in synapses of *pcdh15* mutant photoreceptors. Cell death does not accompany these defects at early stages, suggesting that photoreceptor structural defects, rather than overt cell loss, may underlie vision deficits. Thus, we present the first genetic animal model of a *pcdh15*-associated retinopathy that can be used to understand the etiology of blindness in USH1.

Introduction

Usher syndrome (USH) is an autosomal recessive condition that results in progressive deafness and blindness. Three clinical subtypes of the disease are recognized, and of these USH1 is the most prevalent and severe form (Mathur and Yang, 2015). USH1 is characterized by severe to profound congenital deafness, vestibular defects, and a pre-pubertal onset of retinitis pigmentosa (RP). RP is characterized by progressive primary loss of rod photoreceptors followed by secondary loss of cone photoreceptors (El-Amraoui and Petit, 2014). Mutations in six genes have been linked to USH1 so far. These include the cell adhesion molecules *cadherin-23* (*cdh23*) and *protocadherin-15* (*pcdh15*), scaffolding proteins *harmonin* and *sans*, motor protein *myosin VIIa* and the calcium and integrin binding protein *CIB2* (Mathur and Yang, 2015).

Our understanding of the function of these USH1 genes come primarily from studies in the ear (El-Amraoui and Petit, 2014; Mathur and Yang, 2015). These studies have shown that USH1 proteins function to link together actin-rich microvilli called stereocilia, in neurosensory hair cells of the inner ear. To bridge together adjacent stereocilia, *pcdh15* and *cdh23* interact via the ends of their extracellular cadherin domains to form a structural fiber known as a 'tip link' (Kazmierczak et al., 2007). The other USH1 proteins form an intracellular complex to help anchor the tip links to the F-actin filaments present in the stereocilia (El-Amraoui and Petit, 2014; Mathur and Yang, 2015). When stereocilia are deflected by sound, *pcdh15-cdh23* are stretched, opening physically linked *TMC1/2* channels, causing cellular depolarization (Maeda et al., 2014; Pan et al., 2018). The current model suggests USH1 proteins coordinate tip-link adhesion and tension to regulate auditory mechanotransduction. However, whether USH1 protein dependent adhesion and tension is required for the proper functioning and integrity of photoreceptors are less clear.

USH1 mouse models have aided in our understanding of structural and functional auditory defects associated with the disorder, but most models fail to display retinal defects [reviewed in (El-Amraoui and Petit, 2014)]. Specifically, while some deficiencies in vision have been reported, no mouse mutant has shown retinal degeneration/morphology defects unless exposed to altered light conditions (i.e. enhanced light/lack of pigmentation) (Calabro et al., 2019; Haywood-Watson et al., 2006; Lentz et al., 2010; Libby and Steel, 2001; Libby et al., 2003; Peng et al., 2011; Trouillet et al., 2018; Williams et al., 2009). One possible explanation is that mice exhibit differences in photoreceptor structure that diverge from humans and other species (El-Amraoui and Petit, 2014). For example, USH1 proteins have been found to localize to F-actin

rich microvilli-like protrusive structures, called calyceal processes (CP) that surround outer segments (OS) of photoreceptors (Sahly et al., 2012). CPs appear to be missing from mouse photoreceptors, suggesting that a lack of overt retinopathy in mouse models might be due to species differences. This highlights the need for an accurate and reliable genetic animal model of USH1-associated retinopathy.

Recent knockdowns of *pcdh15* and *cdh23* in *Xenopus* suggest that, like in tip links, *pcdh15-cdh23* structures 'link' CPs to the OS to provide the structural support necessary for proper cone and rod OS shape (Schietroma et al., 2017). Zebrafish photoreceptors have similar CPs (Hodel et al., 2014; Tarboush et al., 2012), yet zebrafish mutant models of various USH1-related genes have shown inconsistent or mild consequences to photoreceptor structure or survival (Glover et al., 2012; Hodel et al., 2014; Phillips et al., 2011; Wasfy et al., 2014). For instance, although *cdh23* is expressed in the zebrafish retina, it has not been detected in photoreceptors, nor have *cdh23* mutants shown defects in the morphology and function of photoreceptors (Glover et al., 2012). Therefore, there is a need for new animal models to decipher the precise function of USH1 related genes in photoreceptors. Additionally, most USH1 gene expression has also been described in photoreceptor synapses, suggesting multiple roles of USH1 proteins may exist, but current analysis has been largely focused on the OS (Reiners et al., 2005).

In this study we focused on *PCDH15* (USH1F), which is associated with up to 20% of USH1 cases (Ouyang et al., 2005; Roux et al., 2006), to generate the first *pcdh15* genetic zebrafish model displaying a clear retinopathy. Zebrafish have two *pcdh15* paralogs: *pcdh15a* and *pcdh15b* (Seiler et al., 2005). Studies of the *pcdh15a* 'orbiter' mutant suggest *pcdh15a* has a

highly conserved function in stereocilia morphology and inner ear hair cell function but no retinal phenotype (Maeda et al., 2017; Seiler et al., 2005). In contrast, *pcdh15b* mRNA is expressed in photoreceptors of the zebrafish embryonic retina, but until now there has been limited evidence for a functional role in the retina (Seiler et al., 2005). We show that *pcdh15* is expressed in the zebrafish retina in photoreceptors at the CPs, inner segment (IS)-OS junction, and synapse. Using loss of function *pcdh15b* mutants generated by CRISPR, we examined the effect on photoreceptors and demonstrate an early, progressively worsening defect in OS morphology and attachment, as well as synaptic disorganization. These structural defects preceded typical signs of photoreceptor cell death. We also found a strong defect in cone morphology, which suggests a distinct etiology compared to a typical RP phenotype previously assumed to underlie the USH1 retinopathy.

Materials and Methods

Zebrafish Husbandry

All strains, including generated mutants, used in this study were derived from the wildtype-AB zebrafish strain background obtained from the Zebrafish International Resource Center (ZIRC) and maintained at our facility at the University of Toronto. *Pcdh15b* mutants generated in-house (see CRISPR Targeting and Genotyping) were kept as heterozygous adults of both male and female sex for breeding and mutant lines were outcrossed for at least two generations before being used for experiments. Unless indicated, all larvae used in the study were the result of in-crossing verified heterozygous male and female adults. All embryos/larvae used for further analysis were genotyped to separate wildtype, heterozygous and homozygous mutant

genotypes from each other. Only mutants verified by genotyping were used for further analysis and siblings genotyped as wildtype (+/+) were used as matched controls. In some cases, WT-ABs obtained from crossings of wildtype adults were also used as additional controls.

In all cases, embryos were collected and grown in a 28^{o}C incubator, in a 100mm wide petri dish containing 40-100 embryos, in the dark until 6 days post fertilization (dpf). In most cases after 6dpf, the larvae were transferred to a 28^{o}C maintained animal facility to receive a 14hr-10hr light-dark cycle (unless in different light treatment groups), fed 0 size food (Gemma Micro 75 zebrafish, Skretting) twice daily (morning and evening) and with water changes twice a day. They were then grown to their desired age. If grown past 10dpf, they were additionally fed brine shrimp in the afternoon. The sex of larvae used in the study is unknown since it is not possible to identify sex of zebrafish at this stage. Animals were treated in accordance with the regulations on animal experimentation established by the Canadian Council on Animal Care (CCAC). The experimental procedures were approved by the University of Toronto Animal Care Committee.

CRISPR Targeting of pcdh15b and Genotyping

Targeting: CRISPR-Cas9 genome editing technology was used to generate mutants for the *pcdh15b* gene in the WT-AB zebrafish background following a protocol previously described (Olsen et al., 2016). A guide RNA (gRNA) targeting the 7th exon of the *pcdh15b* gene with the following sequence, GGGGCTGTTGACATCGATGA, was used to generate mutant founders (Varshney et al., 2013). Briefly, 200pg gRNA (transcribed directly off a long oligonucleotide containing a T7 promoter) and 300pg Cas9 mRNA (transcribed from pT3TS-nCas9n plasmid

(Addgene #46757, RRID:Addgene_46757) were co-injected into the cell of a 1-cell staged embryo and grown to adulthood. The adult founders (F0) were outcrossed and assessed for germline transmission. Those with progeny containing mutations were grown to adulthood (F1) and genotyped by Sanger sequencing for mutations. Two were kept for further analysis, including a 7bp deletion strain (known as Δ7; ZFIN: uot14) and a 17bp insertion strain (known as ins17; ZFIN: uot15). These fish were further outcrossed (F2) and then in-crossed (F3) to obtain homozygous mutants; however, these were not viable as adults. Therefore, heterozygous adults were used for further breeding (see Results). Embryos/larvae used in this study are therefore F4 or older.

Genotyping: All embryos/larvae used in this study were subjected to genotyping. The Δ7 mutants were genotyped by PCR followed by restriction enzyme digestion by ClaI due to the mutation resulting in loss of a ClaI digestion site (which was confirmed by Sanger sequencing). The ins17 mutants were genotyped by Sanger sequencing since the sequence retains the ClaI digestion site. At least 30 or more larvae were genotyped per clutch from multiple clutches for the different experiments. The following primers were used for PCR: F: 5'-AAGAAAGAAAGAACGAAAGAAAGAAA – 3' and R: 5'- GATGGATGGCCATTTGAGAG- 3'.

RT-qPCR

Heterozygous fish were crossed, and embryos were collected. At 10dpf, dissected eyes from individuals (from Δ7 heterozygous crossings) were homogenized into Trizol (Invitrogen #15596018), while the body was used for genotyping. The Trizol solution from individuals were placed at -80^{o}C until genotyping was completed. This was done for greater than 50 individuals

from 3 different clutches (total 150+ embryos). Genotyped embryos were grouped into WT siblings, heterozygous and homozygous mutants yielding 3 groups from 3 different clutches (3 biological replicates). The RNA was extracted from these samples as per the Trizol RNA extraction protocol and eluted into 8uL of nuclease free water. RNA was treated with ezDNase (Invitrogen #11766051), concentration measured using a Nanodrop and then used in Superscript IV First Strand cDNA synthesis (Invitrogen #18090200) in an RT+ and RT- reaction. Eyes dissected from individuals in the ins17 heterozygous crossings (3 different clutches) were treated slightly differently to extract RNA. They were first placed in DNA/RNA shield (Zymogen, R1100), and RNA was extracted from genotyped groups using a column based RNA extraction kit (Zymogen, R1050) before being used for cDNA synthesis with Superscript IV. RNA amounts used in each reaction were calculated to be consistent between samples. qPCR was then performed in technical triplicates using the 3 WT sibling and 3 mutant samples using LightCycler 480 SYBR Green I Master (Roche, #04887352001) with the following primers (note that pcdh15 primers were designed against the beginning third (at around 2000nt) of the mRNA (total 6000-7000nt in length)):

Pcdh15a-F: TTCGCTCAGGTGTCGTACAG

Pcdh15a-R: GACCCCTGGTGCTAAAGTGA

Pcdh15b-F: TAATGACAACACGCCAACCTT

Pcdh15b-R: GCAGCACTGTGATCACTCCT

Actin-F: AAGCAGGAGTACGATGAGTC

Actin-R: TGGAGTCCTCAGATGCATTG

Transmission Electron Microscopy (TEM)

Zebrafish heads were fixed in 2.5% glutaraldehyde in 0.1M phosphate buffer at 4^{o}C overnight or longer, while the tail was used for genotyping (see CRISPR Targeting and Genotyping). After genotyping, the heads were sorted and further processed. Samples were washed out of fixative using 0.1M phosphate buffer (3-4 X 10min) to ensure no trace of glutaraldehyde and placed in 1% osmium tetroxide for 1hr in the dark. Samples were washed out of osmium into 0.1M phosphate buffer and then dehydrated through an ethanol series in 50% (10min), 70% (10min), 80% (15min), 90% (2 X 10min) to 100% (2 X 10 min) ethanol. Samples were then infiltrated with Spurr's epoxy resin through an ethanol: resin series with increasing concentration of resin (of 3:1 for 30min, 1:1 for 30min and 1:3 for 1hr) until they were placed into 100% resin. Resin was allowed to infiltrate the sample tissue overnight, replaced with fresh resin the next day and used for embedding into flat moulds. The resin was allowed to polymerize at 65^{o}C overnight and samples were stored at room temperature until further processed. Sections were cut using a Leica EM UC6 microtome. 1μm semi-thin sections were cut and stained with toluidine blue. Semi-thin sections were imaged on a Leica DMI3000 inverted microscope. 100nm ultrathin sections were cut with a diamond knife and placed on 200-mesh high transmission grid or open-hole slotted grids covered in formvar. Note that slotted grids allowed the whole retina to be visualized and imaged without obstructions. Sections were then stained with 3% uranyl acetate in 50% methanol for 45 minutes and post stained with Reynold's lead citrate for 15min, followed by drying. Samples were imaged using Hitachi HT-7700 at 80kV and images taken with an attached AMT 11-megapixel digital camera.

Scanning Electron Microscopy (SEM)

For analysis of the retina, zebrafish were dark adapted for at least 2 hours before fixation to ensure that retinal pigmented epithelium (RPE) processes were retracted and would not interfere with outer segment visualization. In the dark, anesthetized zebrafish were fixed in 4% paraformaldehyde (PFA) at 4^{o}C overnight. The next day eyes were dissected out and fixed in 2.5% glutaraldehyde in 0.1M phosphate buffer at 4^{o}C overnight, while the body was used for genotyping. For analysis of the lateral line, fish were placed directly in 2.5% glutaraldehyde overnight at 4^{o}C. Samples were sorted by genotype and then processed further. Samples were washed in 0.1M phosphate buffer (3 X 10min), fixed in 1% osmium tetraoxide for 1.5hr in the dark and then washed in 0.1M phosphate buffer (3 X 10min). Samples were dehydrated in ethanol series from 50% to 100% (50%, 70% 80%, 90% and two 100% washes for 10min each) and then placed in ethanol: hexamethyldisilazane (HMDS) series with increasing concentrations of HMDS (3:1, 1:1, 3:1 washes at 10min each) until they were in 100% HMDS (washed 2X 10min). HMDS was allowed to evaporate slowly off the samples in the fume hood overnight. The next day, samples were placed on carbon tape on specimen mounts and sputter coated with gold-palladium for visualization in SEM. For examination of the lateral line, samples were mounted directly. However, for photoreceptor examination in the retina, dried samples were carefully fractured with a blunt ended tool to expose the inner retinal layers and photoreceptor layer, before mounting. Samples were imaged using Hitachi SU3500 at 5kV with a spot intensity of 30.

Whole mount immunofluorescence

Samples, (either heads for inner ear examination or dissected eyes for photoreceptor examination) were fixed in 4% PFA at 4°C no longer than overnight. Samples were sorted by genotype and the next day washed out of fixative in PBST (phosphate buffer saline + 0.8% Triton-X). Samples were permeabilized in ice cold 100% acetone for 10min at -20°C followed by washes in PBST. Samples were additionally permeabilized with proteinase K (20µg/mL) in PBST for 1hr at room temperature. Samples were washed in PBST, post fixed in 4% PFA for 20min at room temperature and washed. Samples were then blocked in saturation buffer (PBST with 10% goat serum and 1% DMSO) for at least 1hr at room temperature. Primary antibody/stain diluted in saturation buffer was incubated for 2-3 days at 4°C with agitation. Samples were then washed 3 times for 1hr each in PBST. If secondary antibody labelling was required, samples were re-blocked in saturation buffer for at least 1 hour, and then placed in diluted secondary antibody overnight. The following day samples were washed in PBST 3-4 times for 1hr each. Before imaging, samples were infiltrated with 80% glycerol for a couple of hours and placed in glass bottom imaging dishes for imaging. Images were taken on a Leica TCSSP8 confocal microscope. The following antibodies/stains were used: Alexa Fluor™ 488 Phalloidin (1:100; ThermoFisher Scientific #A12379), Lectin PNA from *Arachis hypogaea* (peanut) Alexa Fluor™ 488 Conjugate (1:100; ThermoFisher Scientific #L21409, RRID: AB_2315178), Wheat Germ Agglutinin Alexa Fluor™ 555 Conjugate (1:100; W32464), mouse anti-acetylated alpha tubulin (1:500; Sigma, clone 6-11B-1, #T7451, RRID: AB_609894) and Cy3 goat anti-mouse IgG (1:100; Jackson ImmunoResearch Laboratories, 111-165-146, RRID: 2491007).

Immunohistochemistry

Samples were fixed in 4% PFA (in PBS) overnight at 4^{o}C. Samples were cryoprotected by sucrose series of 5 successive 30min washes of increasing sucrose concentration from 5% to 30% sucrose in 1X PBS. Samples were kept overnight in 30% sucrose at 4^{o}C and then exchanged the next day into 2:1 mixture of 30% sucrose: optimal cutting temperature compound (OCT). Samples were frozen at -20^{o}C until sectioning. Cryosections through the heads and eyes were cut at 20 µm thickness. Immunohistochemistry was performed as previously described (Olsen et al., 2016). The following antibodies/stains were used: anti-Caspase-3 (rabbit, 1:200; cleaved (activated), Asp175, Cell Signaling Technologies #9661, RRID: 2341188), anti- Zpr1 (mouse, 1:250, ZIRC), anti-Zpr3 (mouse, 1:250, ZIRC), anti-rhodopsin, clone RET-P1 (mouse, 1:500, Sigma-Aldrich MAB5316), anti-acetylated alpha tubulin (mouse 1:500; Sigma, clone 6-11B-1, #T7451, RRID: AB_609894), Alexa Fluor^{TM} 488 Phalloidin (1:100; ThermoFisher Scientific #A12379), anti-Cacna1fa (1:3000, rabbit; kindly donated by Michael Taylor (Jia et al., 2014)), anti-pcdh15 (1:250, rabbit; NSJ Bioreagents #RQ4652), anti-rabbit Cy3 (Jackson ImmunoResearch Laboratories, #111-165- 003, RRID: AB_2338000), anti-mouse Cy3 (Jackson ImmunoResearch Laboratories, #115-165-146, RRID: 2491007), anti-mouse Cy5 (Jackson ImmunoResearch Laboratories, #115-175-166, RRID: AB_2338714), and anti-rabbit Cy5 (Jackson ImmunoResearch Laboratories, #111-175-144, AB_2338013). Sections were imaged on a Leica TCSSP8 confocal microscope.

Western Blot

Eyes were dissected from individuals obtained from Δ7 heterozygous crossings and immediately frozen at -80°C using an ethanol, dry ice mixture and kept at -80°C until genotyping was completed. The eyes were grouped based on genotype (i.e., wildtype, homozygous mutants) and thawed and homogenized in RIPA buffer (Sigma-Aldrich, R0278) containing fresh protease inhibitor (Sigma-Aldrich, P8340) (98uL RIPA buffer, 2uL protease inhibitor per 100uL) using a pestle, followed by homogenization with a fine needle (27 gauge). The sample was incubated in the extraction mixture for at least 30min at 4°C and then quickly centrifuged to remove debris. Half the sample (equivalent to 14 eyes) was mixed with NuPAGE LDS sample buffer (Invitrogen, NP0007) and 5% β-mercaptoethanol, but not heated prior to being loaded into the gel as this resulted in better results (Tsuji, 2020). The protein samples were run on a NuPAGE 4-12%, Bis-Tris mini protein gel (Invitrogen, NP0335) at 150V for 1 hour. The protein was transferred to a PVDF membrane at a constant current of 200mAmps for about 3hrs/until the largest protein marker (225 kDa) transferred over. The membrane was washed in TBST (20 mM Tris, 150 mM NaCl, 0.05% Tween-20) and then blocked in Blocking solution (5% dried skim milk in TBST) at room temperature for 1 hour. The pcdh15 antibody (NSJ Bioreagents #RQ4652) was diluted in blocking solution at 1:1000 and incubated overnight at 4°C. The membrane was washed in TBST and then incubated with the secondary antibody anti-rabbit HRP (Jackson ImmunoResearch Laboratories #111-035-045, RRID: AB_2337938) at 1:10000 in TBST for 30min at room temperature. The membrane was subsequently washed in TBST. To image, an ECL reaction was performed for 1min (FroggaBio, Ultrascence Western Substrate, #CCH365_Femto) and the membrane was imaged on a ChemiDoc Touch Imaging System (Bio-Rad). The control mouse

anti-actin antibody (EMD Millipore, MAB1501, RRID: AB_2223041) used at 1:10000 was similarly probed and imaged using a anti-mouse HRP secondary antibody (Jackson ImmunoResearch Laboratories #115-035-003, RRID: AB_10015289). The control rabbit anti-H2B antibody (ThermoFisher, PA1-41058, RRID: AB_2118162) used at 1:500 was similarly probed and imaged using a anti-rabbit HRP secondary antibody (Jackson ImmunoResearch Laboratories #111-035-045, RRID: AB_2337938).

Manipulation of light exposure

Prior to 6dpf, all embryos/larvae were treated similarly. At 6dpf, light exposure was manipulated. Lux was measured using a digital lux meter (Dr. Meter) at the level of petri dish placement. In most experiments (excluding the differential light exposure experiments), larvae clutches were moved to the animal facility (kept at 28^{o}C) and were exposed to approximately 250 lux light (un-manipulated light in the facility) on a 14-10hr light-dark cycle until time of sacrifice.

For the differential light exposure experiments, larvae were assigned to different lighting groups. For the 'dark' condition, larvae were covered with a blackout box 24hrs daily. They were only exposed to light during feeding and water changes. For the 'bright light' condition, larvae were placed in the facility under light measuring 500 lux on a 14-10hr light-dark cycle. However, in addition to this light, larvae were exposed to daily periods of white light of 3000 or 6000 lux intensity for 5hrs during the afternoon (12pm-5pm). All groups were exposed to these light treatments from 6-10dpf and then sacrificed.

Experimental Design and Statistical Analysis

Genotyping was performed on > 30 randomly selected larvae to ensure adequate numbers for each experiment. Eyes from at least 4 individuals or more (see the figure captions for more details on number of eyes/animals) were analyzed for each group per experimental procedure and time point.

For immunostaining on sections, 3 consecutive sections in the central retina were examined to ensure consistency across the tissue. For SEM lateral line examination, an average of 5+ neuromasts per individual were used for percentage counts. For SEM retinal examination, at least 5 eyes (from different individuals) were successfully fractured and examined per genotype. For TEM, retinal sections from the central retina (close to the optic nerve) were used for analysis. When possible, both eyes from an individual were analyzed and included in the data. Each dot represents data from one eye (details of number of eyes and individuals examined are in the figure captions). For OS analysis, measurements were taken across the whole retinal section for 4dpf (Δ7, ins17 and controls), 5dpf (Δ7 and controls), 10dpf (Δ7, ins17 and controls) and dark treatment (Δ7 and controls). For 15dpf (Δ7 and controls), and bright light treatment (Δ7 and controls), only the central region of the retinal section, delimited by the plexiform layers, were examined for measurements. The number of OS examined for each measurement are included in the figure captions. For CPs analysis, only the central retina was used. Included in the CP counts were at least 30 OS for each eye. Only CPs that were connected to the OS were included in the count. OS that lacked any CP (i.e., had zero CPs) were not included in the analysis to ensure that we were sampling in a region of the OS where CPs are

consistently observed between genotypes. For synapse analysis, only central retinal synapses were examined (approximately 20-30 synapses per retinal section per individual eye).

Immunostaining data was processed using ImageJ. Hoechst+ cells in the ONL of 3 consecutive confocal sections (20µm each) were counted using IMARIS (Bitplane version 7.7.1, Belfast, United Kingdom). The area was measured using ImageJ and averaged for cells/area in the ONL across the 3 sections. Pyknotic nuclei were counted using ImageJ Cell counter function manually. All TEM measurements were taken on AxioVision SE64 Rel 4.9.1. Statistical analysis and graphs were performed using GraphPad Prism 7.0. Statistical tests used included t-tests (unpaired, two-tailed) when comparing 2 groups or one-way ANOVA when comparing 3 groups. Statistical analysis of the OS morphologies, OS detachment and synapse organization in the different genotypes were done using t-tests. Statistical analysis of time-dependent effects of controls and mutants on photoreceptors and the effect of different light treatments on controls and mutants were done using two-way ANOVA. All error bars represent SD. Specific details about statistical tests can be found in the figure captions.

Results

Pcdh15 is expressed in photoreceptors of the zebrafish retina

We first sought to determine the expression and localization of *pcdh15* in the zebrafish retina. Expression of all USH1 proteins, including *Pcdh15*, in *Xenopus*, macaque, and humans have largely been observed in photoreceptors, and recently described in CPs (Sahly et al., 2012). Within photoreceptors, USH1 proteins have also been described in different regions of the OS, IS and the synapse (Lagziel et al., 2009; Reiners et al., 2003). Moreover, particularly in zebrafish,

expression of *cdh23* and *harmonin* have been described in other retinal cells, such as amacrine cells and Müller glia (Glover et al., 2012; Phillips et al., 2011). To determine *pcdh15* expression in zebrafish, we used a commercially available *pcdh15* antibody designed against the C-terminal region of the protein. This region is present in all described zebrafish pcdh15b isoforms as well as pcdh15a isoforms, with 83% identity to both *pcdh15a* and *pcdh15b* **(Fig. S1A-B**). Expression using this antibody was observed exclusively in photoreceptors at 3dpf and 10dpf (**Figs. 1A & S1C**). We co-labelled with phalloidin, which labels F-actin present in CPs, and found that although *pcdh15* does co-localize with phalloidin-labelled CPs (**Fig. 1A-C, E**), *pcdh15* expression is also found in basolateral regions of the photoreceptor (**Fig. 1A, B, D, F**). Pcdh15 was also found at the IS-OS junction and along the IS plasma membrane (**Fig. 1B, D, F**). Expression was also observed in the presumptive synaptic region of photoreceptors as early as 3dpf, although it does not directly overlap with synaptic actin or SV2, a synaptic vesicle marker at 10dpf **(Figs. 1B, E & S1C**). To determine if *pcdh15* may interact with important synaptic components, we examined the localization of photoreceptor synaptic calcium channel 1.4_{v}, *Cacna1fa*, and found it had minimal overlap with f-actin (**Fig. 1E**). Use of all these markers place *pcdh15* expression immediately adjacent to synaptic components (**Fig. 1E, F**). Therefore, zebrafish *pcdh15* expression is present in CPs, but is also present at the OS base, IS plasma membrane and synapse of the zebrafish photoreceptor. The specificity of the antibody for *pcdh15* is supported by western blot analysis which showed similar sized isoforms to those previously observed in the mouse retina using a C-terminal antibody (Zallocchi et al., 2012) (**Fig. S1D**). The specificity for the *pcdh15b* paralog is supported by an observed reduction in labelling in *pcdh15b* mutant retinas (described below). However, this antibody is expected to recognize both *pcdh15a* and

pcdh15b (see **Fig. S1B**) and therefore this expression pattern may represent a combination of both proteins. In support of this possibility, we examined *pcdh15a* mRNA expression by RT-qPCR and found that it was detected in zebrafish eyes from 3-10dpf at comparable levels of expression to *pcdh15b* (**Fig. S1E & 1I**). These data suggest *pcdh15a/b* proteins are expressed in different sub-compartments of photoreceptors in the zebrafish retina.

CRISPR-generated pcdh15b zebrafish mutants show reduced *pcdh15* staining in the retina and reduced survival

Since *pcdh15a* mutants do not show compromised retinal function, and previous studies suggest *pcdh15b* may have a photoreceptor specific function (Seiler et al., 2005), we aimed to mutate the *pcdh15b* zebrafish paralog by CRISPR gene editing technology. We used a gRNA for *pcdh15b,* targeting a common exon predicted to be present in all alternatively spliced products described thus far. In this case exon 7 was targeted, to ensure most, if not all *pcdh15b* products would be affected (**Fig. 1G**). We identified two mutations for *pcdh15b* which we chose to focus on for further analysis: a 7bp deletion mutant (referred to as Δ7) and a 17bp insertion mutant (referred to as ins17) **(Figs. 1G & S1F-H)**. Both mutations are predicted to severely truncate *pcdh15b* by introducing a premature stop codon in the open reading frame, removing nearly all the extracellular cadherin domain repeats, the transmembrane domain, and the cytoplasmic domain (**Fig. 1H**). Both *pcdh15a* and *pcdh15b* mRNA can be detected in the retina, but no difference in their mRNA levels were observed from the eyes of Δ7 and ins17 mutants (**Fig S1E & 1I)** although we confirmed the mutation was present in the mRNA product by sequencing. In contrast we found that *pcdh15b* mutants had reduced pcdh15 protein expression by immunolabeling, namely along the CPs, cell body and IS-OS base. (**Fig. 1J**). Using the same C-

terminal antibody, we observed a reduction in overall protein levels in mutants by western blot (**Fig. S1D**). Some of the isoforms appeared to be more affected than others, which might correlate with the residual expression we observed by immunolabeling, particularly in the synapse. This is consistent with mouse *Pcdh15* mutants that also demonstrate persistent expression of some isoforms (Alagramam et al., 2011). In addition, our immunolabeling and western blots could be detecting the presence of pcdh15a isoforms.

We observed that homozygous mutants, with either mutant allele, had significantly reduced survival to adulthood (**Fig. 1K**). To analyze this further, we focused on the Δ7 mutants. We genotyped multiple clutches from heterozygous crosses of Δ7 mutants at different time points during development to determine the ratios of each genotype present. We found that all Δ7 mutants die by 20dpf (**Fig. 1K**). Given the comparable phenotypes observed in homozygous mutant larvae from the two separately out-crossed mutant lines, we assume that these phenotypes are specifically associated with a loss of function mutation in *pcdh15b*. Currently, we do not know why homozygous fish die, as we have not identified any overt morphological defects in homozygous fish and feeding behaviour does not seem to be affected. *Pcdh15a* 'orbiter' mutants also have reduced survival (Nicolson et al., 1998), and it has been previously observed that *pcdh15a* and *b* expression are not limited to the ear and retina, respectively (Seiler et al., 2005). Therefore, other ciliated tissues, such as the brain, where *pcdh15b* is highly expressed (Seiler et al., 2005), may be affected in these mutants.

Hair cell defects are not detected in the inner ear and lateral line of *pcdh15b* mutants

Studies have found that *pcdh15* predominately functions at 'tip links' of stereocilia in hair cells to adhere multiple stereocilia into bundled tips (Kazmierczak et al., 2007). In zebrafish, this occurs in hair cells of the inner ear as well as in sensory hair cells along the lateral line, found in structures called neuromasts (Maeda et al., 2017). A 'splayed' degenerative phenotype of tip ends in the ear or neuromasts is commonly observed in *pcdh15a* mutants by 5dpf (Goodman and Zallocchi, 2017; Maeda et al., 2017; Seiler et al., 2005). Similar to *pcdh15a*, some expression of *pcdh15b* has also been previously described in the hair cells of the ear and lateral line (Seiler et al., 2005) but it is unclear if its loss results in a phenotype. We utilized whole mount immunostaining of the inner ear and scanning electron microscopy (SEM) of neuromasts to visualize these bundled tips. After staining and imaging for phalloidin to label F-actin-rich stereocilia in the medial crista of the inner ear, we found that *pcdh15b* mutants showed intact bundled ends, at 5dpf and even 10dpf, suggesting no degenerative phenotype in these cells (**Fig. S2A**). In addition, we found neuromasts showed intact tip ends in our *pcdh15b* mutants comparable to wildtype siblings at 10dpf (**Fig. S2B-C**). Therefore, unlike *pcdh15a* zebrafish mutants and *pcdh15* mouse mutants, our *pcdh15b* zebrafish mutants do not appear to show abnormal hair cell morphology, although we cannot rule out subtle morphological defects. However, unlike *pcdh15a* 'orbiter' mutants which exhibit variable degrees of abnormal 'looping' and 'tilted' swimming (Nicolson et al., 1998), no detectable change in swimming behaviour is observed in our *pcdh15b* mutants (data not shown).

Photoreceptor morphology in *pcdh15b* mutant retinas is abnormal despite no ONL thinning

The lack of retinal phenotypes observed in mouse models of *Pcdh15*- and other associated USH genes has limited our understanding of the retinopathy occurring in this disorder (El-Amraoui and Petit, 2014). According to our protein expression analysis, as well that seen in other species (Sahly et al., 2012; Schietroma et al., 2017), *pcdh15* activity and function appears specific to photoreceptors. However, since other USH1 proteins have been described in other retinal cell types, we first assessed the phenotype of other retinal cell types in our *pcdh15b* mutants and found no overt abnormalities in ganglion cells, amacrine cells or Müller glia at 10dpf (**Fig. S3A, B**).

We next looked more closely at the photoreceptors. Due to the association of USH1 clinical assessments with an RP 'degenerative' phenotype, we hypothesized that *pcdh15* is not necessarily required for photoreceptor development but their maintenance over time and predicted there may be a loss of photoreceptors over time (El-Amraoui and Petit, 2014). However, using the red-green cone cell body marker, Zpr1, we were unable to observe abnormalities in our *pcdh15b* mutants (**Fig S3C).** We examined cell death in the ONL by expression of cleaved (activated) caspase-3 and by the presence of pyknotic nuclei in 10dpf retina and found no difference in the number of caspase3+ cells or pyknotic nuclei in the *pcdh15b* mutants compared to controls (**Fig. 2A-B**). In addition, the density of photoreceptor nuclei was not affected, suggesting there was no ONL thinning (**Fig 2C**). Therefore, these data suggest that death of photoreceptors was not significantly altered in mutants at the stages examined. In zebrafish It is possible that enhanced regeneration of photoreceptors may partially underlie the apparent lack of ONL thinning in diseased or damaged states (Santhanam et al.,

2020; Turkalj et al., 2021; Wan and Goldman, 2016), but given that markers of cell death (apoptosis, pyknotic nuclei) are not observed in any time interval examined we believe this is unlikely.

Next, the outer segment (OS) phenotype previously observed in *Xenopus* knockdowns (Schietroma et al., 2017) lead us to predict that although photoreceptors are still present, they may have abnormalities in their OS. To examine this, we labelled for several different rod and cone OS markers. The cone OS marker, PNA lectin, showed a detectable decrease in size and number in *pcdh15b* mutants at 10dpf onward (**Fig. 2D**). Additionally, the rod OS markers, Zpr3, RET-P1 and WGA-lectin, were all decreased and disorganized in Δ7 mutants (**Figs. 2D & S3C**). Whole mount immunostaining in the 10dpf retina, additionally showed that Δ7 mutants predominately lack proper rod OS staining, particularly in the peripheral retina, although cone OS could still be broadly detected (**Fig. S3E**).

To quantify these differences more precisely, the histology of the photoreceptor layer was closely examined by TEM and used to confirm the abnormalities in the OS. In the wildtype retina, the OS in the photoreceptor layer are typically organized into 2-tiers with an 'inner' and 'outer' row (see **Fig 2E**). The inner row is predominantly made of cone photoreceptor OS and the outer row contains both rod and cone OS (Branchek and Bremiller, 1984; Schmitt and Dowling, 1999). However at 10dpf, the zebrafish retina is mainly composed of cones, with fewer rods present (Branchek and Bremiller, 1984; Raymond et al., 1995). In *pcdh15b* Δ7 and ins17 mutant retinas at 10dpf, the outer segments were disorganized and misshapen, and we observed a significant decrease (>40%) in the number of OS in the inner row (cones) compared to wildtype siblings (**Figs. 2E, F & S3G**). In contrast, the number of OS in the outer row, was not

significantly different (**Fig S3F)**. We observed this specific inner row OS decrease in the Δ7 mutants at both 5dpf and 15dpf, indicating the reduced OS numbers were affected early in photoreceptor development/maturation and were long lasting and not due to a developmental delay (**Figs. 2G & S3G)**. Of the remaining OS in the *pcdh15b* mutants, we also observed a decrease in average OS length compared to wildtype siblings, likely due to the apparent abnormal morphologies of the OS (**Fig 2H**). Together, these results suggest that in the early postembryonic period (up to 20dpf), *pcdh15b* mutant photoreceptors exhibit prominent structural defects that precede any observable cell loss or thinning of the ONL. However, it is possible and likely that these structural OS defects eventually lead to photoreceptor loss classically seen in USH1 patients later in life.

Calyceal processes are formed in *pcdh15b* mutant photoreceptors but have fewer contacts with the outer segment and are lost over time

Previous research, as well as our analysis, has shown that *pcdh15* is localized to the calyceal process (CP) in photoreceptors (Sahly et al., 2012). Furthermore, *pcdh15* knockdown in *Xenopus* results in reduction in the number of CPs (Schietroma et al., 2017). We utilized immunohistochemistry to label F-actin-rich CPs with phalloidin, as well as TEM and SEM to visualize CPs surrounding OS (**Fig. 3A)** to determine how CPs were affected in our *pcdh15b* mutants. Surprisingly, we found phalloidin-labelled CPs were still present in our Δ7 and ins17 mutants at 10dpf, although we noticed a decrease in fluorescence intensity by 15dpf in Δ7 mutants (**Fig. 3B**). This suggested that actin-filled CPs could still form in our *pcdh15b* mutants, although it remained unclear whether they formed adherent structures to the OS. To examine

this further, we performed SEM on retinal tissue, and noticed a reduction of intact CPs surrounding the OS in our *pcdh15b* mutants compared to wildtype siblings (**Fig. 3D**). This suggests CPs have fewer contacts with the OS and may be more prone to detachment. To test this, we visualized CPs by TEM in transverse and horizontal cross-sections. We observed CPs were shorter in length and that there were fewer in *pcdh15b* mutants (**Fig. S4A-C**). We quantified the number of attached CPs per OS in horizontal sections from the central ONL and found that the number of attached CPs in mutants were comparable to wildtype at 4dpf, but that they were significantly reduced by 10dpf, particularly in the ins17 mutants (**Fig. 3C, E**). Interestingly, we also observed evidence of 'detached' CPs in the Δ7 and ins17 mutants (**Figs. 3C & S4D**). These data suggest that CPs in *pcdh15b* mutants are more prone to detachment and eventual loss but initially formed properly. CP loss occurs alongside the observed photoreceptor OS defects described earlier, but whether it contributes to the OS defects or is a consequence of them is difficult to distinguish.

Pcdh15b **mutant retinas exhibit abnormal directional growth of outer segment discs**

To investigate the photoreceptor defects in more detail, we used TEM to analyze the ultrastructure of the OS discs. Previous *pcdh15* knockdown in *Xenopus* suggested two main OS phenotypes: (1) cone OS bending; and (2) basal overgrowth and bulging of rod OS (Schietroma et al., 2017). In contrast, we did not observe any obvious OS bending or enlarged bases of OS (see **Fig. 2D, E**). However, there were clear defects in the canonical 'cone' and 'rod' OS shape (**Fig. 2D, E**). In wildtype sibling retinas, OS discs typically grow horizontal (left to right) and are bounded by the limits of CPs and adjacent photoreceptors. As OS grow, newly formed discs

grow at the base of the OS and result in linearly stacked discs making up the height of an OS (see **Fig. 4A,B**). In contrast, in *pcdh15b* mutants OS discs grew in abnormal directions leading to misshapen OS, likely contributing to the observed decrease in OS length (**Figs. 4A, B & 2H).** Although growth tended to start perpendicular in the mutants, continued growth was often seen apically and even basally orientated. It is important to note that abnormal directional growth occurred in OS that still had contact with CPs, indicating that these growth defects can occur regardless of the presence of CPs. This abnormal growth and morphology occurred in a significantly high percentage of OS in the retina (>50%) of both Δ7 and ins17 mutants and was observed as early as 5dpf (**Fig. 4C-F**). The detection of this defect in the early retina suggests this is likely a developmental rather than degenerative defect. Interestingly, OS in the inner row were more deformed (about 75%) than those in the outer row (50%), also suggesting that cones may be more prone to OS disc growth mis-regulation in these mutants (**Fig. 4C-F**).

Outer segments detach and 'float' away from the photoreceptor cell body in *pcdh15b* mutants

We were interested to know why there was decreased numbers of OS, particularly in the inner row of the photoreceptor layer in *pcdh15b* mutants. Since our data suggested there was no loss of photoreceptor cells, we reasoned instead that OS were 'missing' from their photoreceptor cell bodies. Consistent with this interpretation, we commonly observed 'floating', detached OS, especially in the outer row, significantly more frequently in mutant photoreceptors (**Fig. 5A**, green OS and magenta IS). We reasoned that OS may be more prone to detachment from the photoreceptor cell body due to loss of *pcdh15* expression at the OS base. To observe this phenomenon, we analyzed the inner segment (IS)-OS junction more closely by

TEM. Compared to wildtype siblings, which have proper IS-OS attachments with visible CPs, Δ7 and ins17 mutant photoreceptors showed variable IS-OS connectivity. Some showed retracted or lost CPs, as well as loosening of the OS from the IS (**Fig. 5Bi-iii**) and even complete detachment (**Fig. 5Biv-v, C**). We quantified the percentage of photoreceptor cell bodies lacking any OS connection and found Δ7 and ins17 mutants showed significantly elevated levels of detachment compared to wildtype siblings (close to 50%) at 10dpf and onward (**Fig. 5D**). This detachment was seen as early as 5dpf but to a lesser degree (25%), suggesting phenotypic severity increases over time **(Fig. 5D)**. Due to the different observed stages of detachment, our data suggests OS start to loosen their connection to the IS, in conjunction with weakening contacts with CPs, followed by eventual detachment resulting in 'floating' OS commonly displaced into the outer row. The displacement into the outer row may be partly responsible for offsetting an observed decrease in OS number in this region, but likely explains the observed decrease of OS present in the inner row. Detached OS may be more prone to eventual loss as they are phagocytosed by RPE (Strauss, 2005).

Photoreceptor defects are developmentally acquired and progressively worsen over time in *pcdh15b* mutants

Given that we observed photoreceptor defects as early as 5dpf, we hypothesized that these defects were due to impaired development of photoreceptor structure rather than degeneration of initially properly formed photoreceptors. To test this hypothesis, we examined the ultrastructure of 4dpf photoreceptors, representing a time point immediately after their differentiation and into their maturation phase of development. In zebrafish, differentiation of

photoreceptors begins around 2.3dpf, with the first OS appearing around 2.5dpf and experiencing the greatest growth until 5dpf (Branchek and Bremiller, 1984; Crespo and Knust, 2018; Sukumaran and Perkins, 2009). Therefore, we chose to examine a timepoint between the initial OS maturation and growth (i.e., 4dpf) and found similar defects in the morphology and organization of photoreceptors to that observed in older retinas (**Fig. 6A**). We also noticed a slight decrease in the length of OS of Δ7 and ins17 mutants compared to wildtype siblings (that is even more apparent at later stages previously described), indicating developmental OS growth defects (**Fig. 6B**). Importantly, we still observed a large percentage of abnormal OS discs (~20-25%) (**Fig. 6C)** and photoreceptor cell bodies with missing or detached OS (~35-40%) at 4dpf in our Δ7 and ins17 pcdh15b mutants (**Fig. 6D**). Combining our data from all the different time points analyzed we noticed an intriguing developmental trend: the mutants displayed significant OS abnormalities and detachment immediately following differentiation that worsened with time (**Fig. 6E, F**). These findings alter our current view that USH1 is primarily a degenerative condition by suggesting that photoreceptors may instead develop abnormally with worsening morphological consequences over time as the eye continues to mature.

Exposure to different light intensity can attenuate or exacerbate photoreceptor defects in *pcdh15b* mutants

The defects we observed indicate that photoreceptor OS is severely affected in *pcdh15b* mutant retinas. However, we wondered whether different environmental light conditions could attenuate or exacerbate these defects. This is because, although USH mouse and zebrafish models show mild to no retinal phenotype, increased light exposure has been shown to result in

heightened damage in photoreceptors of mutants (Dona et al., 2018; Peng et al., 2011; Trouillet et al., 2018; Wasfy et al., 2014). In addition, light-dark cycles are necessary for OS turnover (Besharse et al., 1977a; Besharse et al., 1977b) and in the zebrafish retina, changes in this cycle have been seen to effect the growth of OS (Crespo and Knust, 2018). We hypothesized that since OS disc growth and basal OS connection to the IS are defective in the mutants, the severity of these phenotypes is related to continuous OS turnover and therefore could be modulated by light exposure. To answer this question, we exposed our developing zebrafish larvae to either complete darkness (0 lux) or a normal 14/10hr light-dark cycle with 5-hr periods of heightened bright light (3000/6000 lux) daily from 6-10dpf (**Fig. S5A, B**). Interestingly, darkness attenuated the severity of the photoreceptor defects, whereas bright light conditions exacerbated the defects (**Fig. S5A, B**). In particular, the number of OS detected in the inner row was reduced further in bright light conditions compared to dark conditions in Δ7 mutants (**Fig. S5C**). However, this was not a consequence of elevated cell death/ONL thinning in the photoreceptor layer in mutants under bright light (**Fig S5D, E).**

We examined the differential light treated photoreceptors in more detail by TEM and made several interesting observations (**Fig. 7A**). First, although we found the number of inner row OS was reduced in each condition, when normalized to the amount of total OS in both rows, darkness eliminated this decrease, whereas this effect was enhanced in bright light conditions, indicating bright light exacerbates inner OS loss in mutants (**Fig. 7B).** We additionally found that bright light enhanced the percentage of deformed OS in Δ7 mutants, specifically in the inner row, suggesting a strong effect on cone photoreceptors (**Fig. 7C-D).** This enhanced deformity likely contributes to the exacerbated decrease in average OS length we observed

under bright conditions only in the mutants (**Fig. 7E).** The strongest effect we observed was an almost doubling of OS detachment from the photoreceptor cell body/IS in Δ7 mutants under bright conditions compared to dark conditions (**Fig. 7F).** Interestingly, phalloidin labelled CPs were largely still present in mutants under bright conditions, although they looked more disorganized (**Fig. 7G**). However, by TEM, we did notice a decrease in intact CPs (data not shown). This suggests that differential light exposure can reduce or enhance *pcdh15*-associated retinopathic phenotypes.

Increased disorganization of photoreceptor ribbon synapses in *pcdh15b* mutants

Aside from the OS, localization of *pcdh15* and other USH-related proteins have been observed in the synapse of inner hair cells and photoreceptors (Reiners et al., 2005; Zallocchi et al., 2012). However, few studies have investigated the role of USH-proteins in these specialized ribbon synapses. Of the USH-related proteins, type 3 protein, Clarin1 has been most strongly linked to the synapse and to proper synaptic structure in auditory hair cells (Dulon et al., 2018). Given that *pcdh15-cdh23* have been linked to the actin cytoskeleton, we hypothesized that *pcdh15* may play a role in establishing synaptic organization, although it has never been investigated (Cosgrove and Zallocchi, 2014; Dulon et al., 2018). To analyze this, we used TEM to quantify synaptic structure of synapses in the central retina at 5dpf and 10dpf (Allwardt et al., 2001; Schmitt and Dowling, 1999). We found synapses contained all necessary synaptic ribbon components including anchored ribbons, tethered vesicles, bipolar and horizontal cell innervation but that the synapses were increasingly disorganized in Δ7 mutants at 5dpf and 10dpf (**Fig. 8A-C**). Unlike canonical synapses of rods and cones, characterized by medial bipolar

cell innervations surrounded by larger horizontal cell innervations, disorganized synapses commonly had displaced and dispersed innervations (**Fig. 8A, B**). Additionally, we noticed there was a significant decrease in the number of synapses with 2 ribbons or more at 10dpf in Δ7 mutants (**Fig. 8D**)**.** Rod synapses are generally characterized by having 1 ribbon, whereas cones contain multiple ribbons. Therefore, in addition to evidence of disorganized synapses, there appears to be an overall decrease in the percentage of synapses with cone-like features. We wondered whether the disorganization would be reflected in the presence of synaptic proteins and therefore assayed the localization of the photoreceptor synapse calcium channel, $Ca_v1.4$ (*Cacna1fa*) (Jia et al., 2014). At 10dpf, we observed diffuse, smaller puncta staining in Δ7 mutants compared to wildtype siblings (**Fig. 8E**). Given the localization of *pcdh15* expression in the photoreceptor synapse of zebrafish, *pcdh15* may interact with synaptic components that connect to F-actin filaments, but the exact mechanism is unclear. Overall, our data suggests that *pcdh15b* is necessary to maintain photoreceptor synaptic organization.

Discussion

We present one of the first genetic animal mutants for *pcdh15* that displays a severe, early retinopathy and suggests that zebrafish could be a useful model for USH1F-associated retinal phenotypes. Our findings demonstrate that *pcdh15b* function is required in three main subcellular compartments in photoreceptors: CPs, the IS-OS junction, and the synapse (**Fig S6A-D**). Specifically, we found that in our mutants CPs maintain fewer contacts with OS, resulting in OS disc growth misdirection, especially in cone photoreceptors. In agreement with Schietroma et al., 2017, our data suggests that *pcdh15b* attaches CPs to OS, but we note that *pcdh15b* does

not appear to be required for initial CP formation, but rather to stabilize the connection of CPs to OS over time (**Fig. S6B**). Secondly, we found that photoreceptor structural integrity was compromised resulting in severe detachment of OS from the IS. This suggest *pcdh15b* expression at the IS-OS junction functions to anchor the basal discs to the plasma membrane of the IS (**Fig. S6C**). Lastly, we found disorganization of synaptic components, suggesting *pcdh15b* is required for proper synaptic architecture (**Fig. S6D**), possibly by linking synaptic components to the F-actin network. Interestingly all these effects were found as early as 4dpf suggesting these defects are developmentally acquired. We also show that *pcdh15b* zebrafish mutants have selective defects in photoreceptors of the retina but not cells of the ear, providing the unique opportunity to study retinal specific defects of USH1F. Nonetheless, one of the limitations of this mutant is that they are larval lethal, which inevitably limits longer term studies. Understanding what additional systemic defects occur that lead to death or the creation of conditional retinal knockouts could be useful if longer term studies are desired.

Pcdh15b **function in calyceal processes**

Our current model refines the previous model proposed for *pcdh15* and other associated USH1 proteins at CPs (Sahly et al., 2012; Schietroma et al., 2017). The previous model supported by *Xenopus* studies suggested that USH1 proteins function in CPs to stabilize and prevent bending of cone OS and limit basal OS disc growth in rods (Schietroma et al., 2017). We do not observe cone OS bending, but instead notice extensive abnormal directional growth of OS discs in rods, and especially in cones, given the highly cone dominant zebrafish retina. Thus, we posit that the main function of USH1-associated proteins in CPs is to link to the ends of OS discs to

control/limit their growth. It is possible that the differences seen between *Xenopus* and zebrafish may in part be due to differences in methods (knockdown vs mutant analysis; or, timing of analysis), inherent differences in photoreceptor density and composition between *Xenopus* (rod-dominant; similar to mice) and zebrafish retinas (cone-dominant) (Gábriel and Wilhelm, 2001; Noel et al., 2021; Roehlich and Szel, 2000), and the partial functional compensation of *pcdh15a* in zebrafish retinas. However, evidence for a role for *pcdh15a* in the retina is limited (Seiler et al., 2005), and more research is required.

Interestingly, studies of a mutation in a retinal specific gene, protocadherin21 (*Pcdh21*), which belongs to a subset of cadherins structurally similar to *Cdh23* and *Pcdh15* (Elledge et al., 2010), report morphological defects that are similar to those reported here. *Pcdh21* is expressed at the base of photoreceptors, where it links open lamellar evaginations of discs in rods and cones to the opposing IS membrane (Burgoyne et al., 2015). Knockout of *Pcdh21* in mice results in abnormal disc organization and morphogenesis, similar to our mutants, and leads to eventual photoreceptor degeneration (Rattner et al., 2001). Additionally, loss of *prominin1*, a known *pcdh21* interacting protein expressed at the base of OS, also results in OS discs displaying abnormal directional growth, similar to our mutants (Lu et al., 2019; Yang et al., 2008). With this model, the differences between rod and cone structure can account for increased severity we notice in cones. Rods are encapsulated by an outer plasma membrane that only leaves basally located newly forming lamella exposed. Conversely, cone OS discs are made entirely of open lamella evaginations and only have CPs to tether onto for structural stability (Bujakowska et al., 2017; Goldberg et al., 2016; Steinberg et al., 1980). It is notable that mutations in human *PCDH21* are associated with cone-rod dystrophy and retinal degeneration

(Henderson et al., 2010; Ostergaard et al., 2010), but an association of *PCDH15* or other USH1 proteins with cone-rod dystrophy is, however, unclear. Therefore, *pcdh15*-attached CPs must be especially important for cone OS disc growth, explaining why cones are more prone to deformation in our *pcdh15b* mutants. It is not clear why only a subset of OS is affected in our mutants (i.e., 50%-75%), but it seems plausible that in addition to potential rod and cone differences, the phenotype is age dependent as we see defects get worse over time. It is also possible that there is some, perhaps variable, compensation by *pcdh15a*.

According to this model, *pcdh15* is functioning similarly, as in the inner ear, to 'adhere' structures together. However, in the ear the physical length and elasticity/tension created by *pcdh15-cdh23* links in stereocilia and in response to deflection has a clear functional role in mechanotransduction (Dionne et al., 2018; Jaiganesh et al., 2018). Whether photoreceptors require molecules with these physical properties is unclear. Furthermore, it is not known whether the *cdh23-pcdh15* interaction is conserved in the zebrafish retina, due to the lack of *cdh23* expression observed in photoreceptors (Glover et al., 2012). If not, is it possible that *pcdh15* forms a homophilic interaction to mediate adhesive connections in the structures of the photoreceptor? This is unknown and needs to be further tested biochemically, but combinations of alternatively spliced *pcdh15* molecules that form a pseudo-heterophilic tip link may be possible (Narui and Sotomayor, 2018). Another question raised is why elasticity and tension created by these molecules would be required in photoreceptors. It is possible that the dynamic nature of apical shedding and basal growth of newly formed discs in photoreceptors (Goldberg et al., 2016; Willoughby and Jensen, 2012) require elastic forces to maintain structural integrity. This may explain why different light exposures, that may affect the dynamic

growth of OS, change the severity of the phenotype. Studies mimicking known mutations that reduce elasticity of the *pcdh15* while maintaining other *pcdh15* structural properties (Bartsch et al., 2019) in the retina can be examined. Testing whether similar defects to our mutants are observed or not with these specific mutations can determine if these physical properties are important for vision. Moreover, our western blot analysis, along with others (Zallocchi et al., 2012) indicates multiple isoforms of different sizes are expressed in the retina, suggesting the possibility that the retina requires some pcdh15 molecules with different properties.

Pcdh15b depletion causes loss of OS prior to overt photoreceptor cell death

Our results suggest *pcdh15*b has additional functions in the photoreceptor. First, *pcdh15b* appears to be necessary to connect the base of the OS to the inner segment. Loss of this connection may put additional strain on the connecting cilium and axoneme resulting in eventual breakage and complete detachment. Previous USH1 studies exclusively look for retinal thinning or markers of cell death to establish a retinal phenotype in animal models (Glover et al., 2012; Libby et al., 2003; Peng et al., 2011; Wasfy et al., 2014; Williams et al., 2009). Although it is possible, and even likely, that OS loss leads to cell death, our results suggest OS loss precedes any observable loss in photoreceptors. Intriguingly, this may suggest early treatment focused on stabilizing OS biogenesis, or initiating it de novo, rather than replacement of lost photoreceptors may be a more beneficial approach for USH1 therapy before widespread death (Horton et al., 2015).

How does *pcdh15b* loss of function lead to OS defects? Our data suggest that unlike what was previously proposed, CP loss is not the primary defect. This is because CPs appear to form and are only observed to decrease by 10dpf, a time point in which other defects are already evident. Therefore, we propose a model in our mutants where CPs are formed normally, but they are improperly connected (or lack connection) to OS. This allows OS to grow beyond or away from CP boundaries as they fail to form a proper disc-CP attachment over time (**Fig. S6E**). Eventually the OS discs also loses attachment to the IS, as OS turn over and put additional strain on the connecting cilium/axoneme to break off entirely, leaving CPs to eventually retract (**Fig. S6E**).

Pcdh15b and synapse organization

Our results also suggest *pcdh15b* function is required at the photoreceptor synapse. Expression data of USH1 proteins has shown that all proteins, albeit possibly as different, and even shorter isoforms, are present at photoreceptor synapses, suggesting it is a main site of USH1 function (Reiners et al., 2006). Both the long full length and shortened isoforms (likely missing the extracellular domain) of *Pcdh15* have been described in the synapse (Alagramam et al., 2011) and our data suggest that the shorter isoforms are likely still expressed in our mutant. Therefore, although we do see clear organizational defects, complete disruption of *pcdh15b* function in the synapse may not be fully reflected from our mutant.

Clarin-1, a type 3 USH protein, has the strongest functional link to synapses in hair cells so far. Loss of *Clarin-1* results in delays in synaptic maturation (Ogun and Zallocchi, 2014; Zallocchi et al., 2012), and in abnormal clustering of calcium channels, $Ca_v1.3$ at the active zones of ribbons of inner hair cells leading to lower calcium efficiency of exocytosis (Dulon et al., 2018). Disruption and loss of organized synaptic actin networks due to *Clarin-1* loss are also observed (Dulon et al., 2018), suggesting actin maintains tight spatial organization of $Ca_v1.3$ necessary for excitatory transmission (Vincent et al., 2015). Similar connection to synaptic activity and synaptic F-actin has been observed for USH2 gene, Whirlin (Jepson et al., 2014; Kersten et al., 2010). In photoreceptors, tight spatial control of $Ca_v1.4$ beneath the synaptic ribbon is regulated by actin (Mercer et al., 2011). It has also been previously observed that *Clarin-1* physically interacts with *pcdh15a* in zebrafish hair cells (Ogun and Zallocchi, 2014). Therefore, in agreement with previous data, our results link *pcdh15b* in zebrafish photoreceptors to synaptic organization and $Ca_v1.4$ localization which may impact synaptic function. This disorganization in the mutant occurs early and occurs as the synapse is developing (**Fig. S6E**). However, the exact protein interactions of *pcdh15b* with other USH1 or other synaptic components responsible remain poorly understood.

Clinical features of retinitis pigmentosa associated with PCDH15 mutation

Although our mutants display a severe retinopathy, the heightened severity in cones is atypical for RP, the primary retinal prognosis in USH patients. In addition, we show that the defects can be exacerbated in cones but not rods under bright light. However, rods clearly show defects in our mutants as well. To date, no cases associated with *PCDH15* mutations have been

described as a cone-rod dystrophy. Clinical data among USH1 cases though, are variable in their progression, and some cases have been associated with colour blindness related defects including Tritan defect and severe dyschromatopsia (Khateb et al., 2019; Mrugacz M et al., 2010). In addition, studies of albino *harmonin* and *sans* knockout mice show primary degeneration of cones (Trouillet et al., 2018). A recently identified USH-like causative gene, *CEP290*, is also associated with cone-rod dystrophy (Fuster-García et al., 2018).

Our data suggest that *PCDH15* and other USH1 gene mutations may present progression of features atypical of RP. The early onset of photoreceptor defects in our mutants also highlight that causes of RP for USH1 may be due to improper development of photoreceptor OS and synapses rather than later onset degeneration in young children/adolescents typically seen for USH1-related RP. These phenotypes may prove useful in 'early' diagnosis of USH1 associated retinal defects before the onset of blindness. Furthermore, it might be possible to utilize our *pcdh15b* mutants in chemical screens to identify known or novel compounds that ameliorate the photoreceptor defects. Lastly, the retinal specific consequences found in our *pcdh15b* mutants, and not in *pcdh15a* mutants (Seiler et al., 2005), may provide insight into why particular mutations in *PCDH15* are only associated with non-syndromic deafness, whereas others lead to USH1 (Ahmed et al., 2008).

References

Ahmed, Z. M., Riazuddin, S., Aye, S., Ali, R. A., Venselaar, H., Anwar, S., Belyantseva, P. P., Qasim, M., Riazuddin, S. and Friedman, T. B. (2008). Gene structure and mutant alleles of PCDH15: Nonsyndromic deafness DFNB23 and type 1 Usher syndrome. *Hum. Genet.* **124**, 215–223.

Alagramam, K. N., Goodyear, R. J., Geng, R., Furness, D. N., Aken, A. F. J. van, Marcotti, W., Kros, C. J. and Richardson, G. P. (2011). Mutations in Protocadherin 15 and Cadherin 23 Affect Tip Links and Mechanotransduction in Mammalian Sensory Hair Cells. *PLoS One* **6**, e19183.

Allwardt, B. A., Lall, A. B., Brockerhoff, S. E. and Dowling, J. E. (2001). Synapse formation is arrested in retinal photoreceptors of the zebrafish nrc mutant. *J. Neurosci.* **21**, 2330–2342.

Bartsch, T. F., Hengel, F. E., Oswald, A., Dionne, G., Chipendo, I. V., Mangat, S. S., Shatanofy, M. El, Shapiro, L., Müller, U. and Hudspeth, A. J. (2019). Elasticity of individual protocadherin 15 molecules implicates tip links as the gating springs for hearing. *Proc. Natl. Acad. Sci. U. S. A.* **166**, 11048–11056.

Besharse, J. C., Hollyfield, J. G. and Rayborn, M. E. (1977a). Photoreceptor outer segments: Accelerated membrane renewal in rods after exposure to light. *Science (80-.).* **196**, 536–538.

Besharse, J. C., Hollyfield, J. G. and Rayborn, M. E. (1977b). Turnover of rod photoreceptor outer segments: II. membrane addition and loss in relationship to light. *J. Cell Biol.* **75**, 507–527.

Branchek, T. and Bremiller, R. (1984). The development of photoreceptors in the zebrafish,Brachydanio rerio. I. Structure. *J. Comp. Neurol.* **224**, 107–115.

Bujakowska, K. M., Liu, Q. and Pierce, E. A. (2017). Photoreceptor cilia and retinal ciliopathies. *Cold Spring Harb. Perspect. Biol.* **9**, a028274.

Burgoyne, T., Meschede, I. P., Burden, J. J., Bailly, M., Seabra, M. C. and Futter, C. E. (2015). Rod disc renewal occurs by evagination of the ciliary plasma membrane that makes cadherin-based contacts with the inner segment. *Proc. Natl. Acad. Sci. U. S. A.* **112**, 15922–15927.

Calabro, K. R., Boye, S. L., Choudhury, S., Fajardo, D., Peterson, J. J., Li, W., Crosson, S. M., Kim, M. J., Ding, D., Salvi, R., et al. (2019). A Novel Mouse Model of MYO7A USH1B Reveals Auditory and Visual System Haploinsufficiencies. *Front. Neurosci.* **13**, 1255.

Cosgrove, D. and Zallocchi, M. (2014). Usher protein functions in hair cells and photoreceptors. *Int. J. Biochem. Cell Biol.* **46**, 80–89.

Crespo, C. and Knust, E. (2018). Characterisation of maturation of photoreceptor cell subtypes during zebrafish retinal development. *Biol. Open* **7**, bio036632.

Dionne, G., Qiu, X., Rapp, M., Liang, X., Zhao, B., Peng, G., Katsamba, P. S., Ahlsen, G., Rubinstein, R., Potter, C. S., et al. (2018). Mechanotransduction by PCDH15 Relies on a Novel cis-Dimeric Architecture. *Neuron* **99**, 480-492.e5.

Dona, M., Slijkerman, R., Lerner, K., Broekman, S., Wegner, J., Howat, T., Peters, T., Hetterschijt, L., Boon, N., De Vrieze, E., et al. (2018). Usherin defects lead to early-onset retinal dysfunction in zebrafish HHS Public Access. *Exp Eye Res* **173**, 148–159.

Dulon, D., Papal, S., Patni, P., Cortese, M., Vincent, P. F. Y., Tertrais, M., Emptoz, A., Tlili, A., Bouleau, Y., Michel, V., et al. (2018). Clarin-1 gene transfer rescues auditory synaptopathy in model of Usher syndrome. *J. Clin. Invest.* **128**, 3382–3401.

El-Amraoui, A. and Petit, C. (2014). The retinal phenotype of Usher syndrome: Pathophysiological insights from animal models. *Comptes Rendus - Biol.* **337**, 167–177.

Elledge, H. M., Kazmierczak, P., Clark, P., Joseph, J. S., Kolatkar, A., Kuhn, P. and Müller, U. (2010). Structure of the N terminus of cadherin 23 reveals a new adhesion mechanism for a subset of cadherin superfamily members. *Proc. Natl. Acad. Sci. U. S. A.* **107**, 10708–10712.

Fuster-García, C., García-García, G., Jaijo, T., Fornés, N., Ayuso, C., Fernández-Burriel, M., Sánchez-De la Morena, A., Aller, E. and Millán, J. M. (2018). High-throughput sequencing for the molecular diagnosis of Usher syndrome reveals 42 novel mutations and consolidates CEP250 as Usher-like disease causative. *Sci. Rep.* **8**, 17113.

Gábriel, R. and Wilhelm, M. (2001). Structure and function of photoreceptor and second-order cell mosaics in the retina of Xenopus. *Int. Rev. Cytol.* **210**, 77–120.

Glover, G., Mueller, K. P., Söllner, C., Neuhauss, S. C. F. and Nicolson, T. (2012). The Usher gene cadherin 23 is expressed in the zebrafish brain and a subset of retinal amacrine cells. *Mol. Vis.* **18**, 2309–2322.

Goldberg, A. F., Moritz, O. L. and Williams, D. S. (2016). Molecular basis for photoreceptor outer segment architecture. *Prog. Retin. Eye Res.* **55**, 52–81.

Goodman, L. and Zallocchi, M. (2017). Integrin α8 and Pcdh15 act as a complex to regulate cilia biogenesis in sensory cells. *J. Cell Sci.* **130**, 3698–3712.

Haywood-Watson, R. J. L., Ahmed, Z. M., Kjellstrom, S., Bush, R. A., Takada, Y., Hampton, L. L., Battey, J. F., Sieving, P. A. and Friedman, T. B. (2006). Ames waltzer deaf mice have reduced electroretinogram amplitudes and complex alternative splicing of Pcdh15 transcripts. *Investig. Ophthalmol. Vis. Sci.* **47**, 3074–3084.

Henderson, R. H., Li, Z., Abd El Aziz, M. M., Mackay, D. S., Eljinini, M. A., Zeidan, M., Moore, A. T., Bhattacharya, S. S. and Webster, A. R. (2010). Biallelic mutation of protocadherin-21 (PCDH21) causes retinal degeneration in humans. *Mol. Vis.* **16**, 46–52.

Hodel, C., Niklaus, S., Heidemann, M., Klooster, J., Kamermans, M., Biehlmaier, O., Gesemann, M. and Neuhauss, S. C. F. (2014). Myosin VIIA is a Marker for the Cone Accessory Outer Segment in Zebrafish. *Anat. Rec.* **297**, 1777–1784.

Horton, J. C., Parker, A. B., Botelho, J. V. and Duncan, J. L. (2015). Spontaneous Regeneration of Human Photoreceptor Outer Segments. *Sci. Rep.* **5**, 12364.

Jaiganesh, A., Narui, Y., Araya-Secchi, R. and Sotomayor, M. (2018). Beyond cell–cell adhesion: Sensational cadherins for hearing and balance. *Cold Spring Harb. Perspect. Biol.* **10**, a029280.

Jepson, J. E. C., Shahidullah, M., Liu, D., le Marchand, S. J., Liu, S., Wu, M. N., Levitan, I. B., Dalva, M. B. and Koh, K. (2014). Regulation of synaptic development and function by the Drosophila PDZ protein Dyschronic. *Dev.* **141**, 4548–4557.

Jia, S., Muto, A., Orisme, W., Henson, H. E., Parupalli, C., Ju, B., Baier, H. and Taylor, M. R. (2014). Zebrafish Cacna1fa is required for cone photoreceptor function and synaptic ribbon formation. *Hum. Mol. Genet.* **23**, 2981–2994.

Kazmierczak, P., Sakaguchi, H., Tokita, J., Wilson-Kubalek, E. M., Milligan, R. A., Müller, U. and Kachar, B. (2007). Cadherin 23 and protocadherin 15 interact to form tip-link filaments in sensory hair cells. *Nature* **449**, 87–91.

Kersten, F. F. J., van Wijk, E., van Reeuwijk, J., van der Zwaag, B., Märker, T., Peters, T. A., Katsanis, N., Wolfrum, U., Keunen, J. E. E., Roepman, R., et al. (2010). Association of whirlin with Cav1.3 (α1D) channels in photoreceptors, defining a novel member of the usher protein network. *Investig. Ophthalmol. Vis. Sci.* **51**, 2338–2346.

Khateb, S., Mohand-Saïd, S., Nassisi, M., Bonnet, C., Roux, A.-F., Andrieu, C., Antonio, A., Condroyer, C., Zeitz, C., Devisme, C., et al. (2019). Phenotypic characteristics of rod-cone dystrophy associated with MYO7A mutations in a large French cohort. *Retina* **Advance on**, 10.1097.

Lagziel, A., Overlack, N., Bernstein, S. L., Morell, R. J., Wolfrum, U. and Friedman, T. B. (2009). Expression of cadherin 23 isoforms is not conserved: implications for a mouse model of Usher syndrome type 1D. *Mol. Vis.* **15**, 1843–57.

Lentz, J. J., Gordon, W. C., Farris, H. E., Macdonald, G. H., Cunningham, D. E., Robbins, C. A., Tempel, B. L., Bazan, N. G., Rubel, E. W., Oesterle, E. C., et al. (2010). Deafness and Retinal Degeneration in A Novel USH1C Knock-In Mouse Model. *Dev Neurobiol* **70**, 253–267.

Libby, R. T. and Steel, K. P. (2001). Electroretinographic anomalies in mice with mutations in Myo7a, the gene involved in human Usher syndrome type 1B. *Investig. Ophthalmol. Vis. Sci.* **42**, 770–778.

Libby, R. T., Kitamoto, J., Holme, R. H., Williams, D. S. and Steel, K. P. (2003). Cdh23 mutations in the mouse are associated with retinal dysfunction but not retinal degeneration. *Exp. Eye Res.* **77**, 731–739.

Lu, Z., Hu, X., Reilly, J., Jia, D., Liu, F., Yu, S., Liu, X., Xie, S., Qu, Z., Qin, Y., et al. (2019). Deletion of the transmembrane protein Prom1b in zebrafish disrupts outer-segment morphogenesis and causes photoreceptor degeneration. *J. Biol. Chem.* **294**, 13953–13963.

Maeda, R., Kindt, K. S., Mo, W., Morgan, C. P., Erickson, T., Zhao, H., Clemens-Grisham, R., Barr-Gillespie, P. G. and Nicolson, T. (2014). Tip-link protein protocadherin 15 interacts with transmembrane channel-like proteins TMC1 and TMC2. *Proc. Natl. Acad. Sci. U. S. A.* **111**, 12907–12912.

Maeda, R., Pacentine, I. V., Erickson, T. and Nicolson, T. (2017). Functional analysis of the transmembrane and cytoplasmic domains of Pcdh15a in zebrafish hair cells. *J. Neurosci.* **37**, 3231–3245.

Mathur, P. and Yang, J. (2015). Usher syndrome: Hearing loss, retinal degeneration and associated abnormalities. *Biochim. Biophys. Acta - Mol. Basis Dis.* **1852**, 406–420.

Mercer, A. J., Chen, M. and Thoreson, W. B. (2011). Lateral mobility of presynaptic L-Type calcium channels at photoreceptor ribbon synapses. *J. Neurosci.* **31**, 4397–4406.

Mrugacz M, M, S. and Sredzińska-Kita D, B.-Ł. A. (2010). Estimation of morphology and function of the eye in Usher's syndrome. *Klin Ocz.* **112**, 324–327.

Narui, Y. and Sotomayor, M. (2018). Tuning inner ear tip link affinity through alternatively splaced variants of protocadherin-15. *Physiol. Behav.* **176**, 139–148.

Nicolson, T., Rüsch, A., Friedrich, R. W., Granato, M., Ruppersberg, J. P. and Nüsslein-Volhard, C. (1998). Genetic analysis of vertebrate sensory hair cell mechanosensation: The zebrafish circler mutants. *Neuron* **20**, 271–283.

Noel, N. C. L., Macdonald, I. M. and Allison, W. T. (2021). Zebrafish models of photoreceptor dysfunction and degeneration. *Biomolecules* **11**, 1–33.

Ogun, O. and Zallocchi, M. (2014). Clarin-1 acts as a modulator of mechanotransduction activity and presynaptic ribbon assembly. *J. Cell Biol.* **207**, 375–391.

Olsen, J. B., Wong, L., Deimling, S., Miles, A., Guo, H., Li, Y., Zhang, Z., Greenblatt, J. F., Emili, A. and Tropepe, V. (2016). G9a and ZNF644 Physically Associate to Suppress Progenitor Gene Expression during Neurogenesis. *Stem Cell Reports* **7**, 454–470.

Ostergaard, E., Batbayli, M., Duno, M., Vilhelmsen, K. and Rosenberg, T. (2010). Mutations in PCDH21 cause autosomal recessive cone-rod dystrophy. *J. Med. Genet.* **47**, 665–669.

Ouyang, X. M., Yan, D., Li, A. E., Du, L., Fielding, J., Ae, H., Jacobson, S. G., Ae, W. E. N., Ren, A., Ae, L., et al. (2005). Characterization of Usher syndrome type I gene mutations in an Usher syndrome patient population. *Hum. Genet.* **116**, 292–299.

Pan, B., Akyuz, N., Liu, X. P., Asai, Y., Nist-Lund, C., Kurima, K., Derfler, B. H., György, B., Limapichat, W., Walujkar, S., et al. (2018). TMC1 Forms the Pore of Mechanosensory Transduction Channels in Vertebrate Inner Ear Hair Cells. *Neuron* **99**, 736-753.e6.

Peng, Y. W., Zallocchi, M., Wang, W. M., Delimont, D. and Cosgrove, D. (2011). Moderate Light-Induced Degeneration of Rod Photoreceptors with Delayed Transducin Translocation in shaker1 Mice. *Investig. Ophthalmol. Vis. Sci.* **52**, 6421–6427.

Phillips, J. B., Blanco-Sanchez, B., Lentz, J. J., Tallafuss, A., Khanobdee, K., Sampath, S., Jacobs, Z. G., Han, P. F., Mishra, M., Titus, T. A., et al. (2011). Harmonin (Ush1c) is required in zebrafish Müller glial cells for photoreceptor synaptic development and function. *DMM Dis. Model. Mech.* **4**, 786–800.

Rattner, A., Smallwood, P. M., Williams, J., Cooke, C., Savchenko, A., Lyubarsky, A., Pugh, E. N. and Nathans, J. (2001). A Photoreceptor-Specific Cadherin Is Essential for the Structural Integrity of the Outer Segment and for Photoreceptor Survival. *Neuron* **32**, 775–786.

Raymond, P. A., Barthel, L. K. and Curran, G. A. (1995). Developmental patterning of rod and cone photoreceptors in embryonic zebrafish. *J. Comp. Neurol.* **359**, 537–550.

Reiners, J., Reidel, B., El-Amraoui, A., Boëda, B., Huber, I., Petit, C. and Wolfrum, U. (2003). Differential Distribution of Harmonin Isoforms and Their Possible Role in Usher-1 Protein Complexes in Mammalian Photoreceptor Cells. *Investig. Ophthalmol. Vis. Sci.* **44**, 5006–5015.

Reiners, J., Märker, T., Jürgens, K., Reidel, B. and Wolfrum, U. (2005). Photoreceptor expression of the Usher syndrome type 1 protein protocadherin 15 (USH1F) and its interaction with the scaffold protein harmonin (USH1C). *Mol. Vis.* **11**, 347–355.

Reiners, J., Nagel-Wolfrum, K., Jürgens, K., Märker, T. and Wolfrum, U. (2006). Molecular basis of human Usher syndrome: Deciphering the meshes of the Usher protein network provides insights into the pathomechanisms of the Usher disease. *Exp. Eye Res.* **83**, 97–119.

Roehlich, P. and Szel, A. (2000). Photoreceptor cells in the Xenopus retina. *Microsc. Res. Tech.* **337**, 327–337.

Roux, A. F., Fougère, V., Le Guédard, S., Pallares-Ruiz, N., Vielle, A., Chambert, S., Marlin, S., Hamel, C., Gilbert, B., Malcolm, S., et al. (2006). Survey of the frequency of USH1 gene mutations in a cohort of Usher patients shows the importance of cadherin 23 and protocadherin 15 genes and establishes a detection rate of above 90%. *J. Med. Genet.* **43**, 763–768.

Sahly, I., Dufour, E., Schietroma, C., Michel, V., Bahloul, A., Perfettini, I., Pepermans, E., Estivalet, A., Carette, D., Aghaie, A., et al. (2012). Localization of usher 1 proteins to the photoreceptor calyceal processes, which are absent from mice. *J. Cell Biol.* **199**, 381–399.

Santhanam, A., Shihabeddin, E., Atkinson, J. A., Nguyen, D., Lin, Y. P. and O'Brien, J. (2020). A Zebrafish Model of Retinitis Pigmentosa Shows Continuous Degeneration and Regeneration of Rod Photoreceptors. *Cells* **9**,.

Schietroma, C., Parain, K., Estivalet, A., Aghaie, A., Boutet de Monvel, J., Picaud, S., Sahel, J.-A., Perron, M., El-Amraoui, A. and Petit, C. (2017). Usher syndrome type 1-associated cadherins shape the photoreceptor outer segment. *J. Cell Biol.* **216**, 1849–1864.

Schmitt, E. A. and Dowling, J. E. (1999). Early retinal development in the zebrafish, Danio rerio: Light and electron microscopic analyses. *J. Comp. Neurol.* **404**, 515–536.

Seiler, C., Finger-Baier, K. C., Rinner, O., Makhankov, Y. V., Schwarz, H., Neuhauss, S. C. F. and Nicolson, T. (2005). Duplicated genes with split functions: Independent roles of protocadherin 15 orthologues in zebrafish hearing and vision. *Development* **132**, 615–623.

Steinberg, R. H., Fisher, S. K. and Anderson, D. H. (1980). *Disc Morphogenesis in Vertebrate Photoreceptors*.

Strauss, O. (2005). The Retinal Pigment Epithelium in Visual Function. *https://doi-org.myaccess.library.utoronto.ca/10.1152/physrev.00021.2004* **85**, 845–881.

Sukumaran, S. and Perkins, B. D. (2009). Early defects in photoreceptor outer segment morphogenesis in zebrafish ift57, ift88 and ift172 Intraflagellar Transport mutants. *Vision Res.* **49**, 479.

Tarboush, R., Chapman, G. B. and Connaughton, V. P. (2012). Ultrastructure of the distal retina of the adult zebrafish, Danio rerio. *Tissue Cell* **44**, 264–279.

Trouillet, A., Dubus, E., Dégardin, J., Estivalet, A., Ivkovic, I., Godefroy, D., García-Ayuso, D., Simonutti, M., Sahly, I., Sahel, J. A., et al. (2018). Cone degeneration is triggered by the absence of USH1 proteins but prevented by antioxidant treatments. *Sci. Rep.* **8**, 1968.

Tsuji, Y. (2020). Transmembrane protein western blotting: Impact of sample preparation on detection of SLC11A2 (DMT1) and SLC40A1 (ferroportin). *PLoS One* **15**, e0235563.

Turkalj, B., Quallich, D., Bessert, D. A., Kramer, A. C., Cook, T. A. and Thummel, R. (2021). Development and characterization of a chronic photoreceptor degeneration model in adult zebrafish that does not trigger a regenerative response. *Exp. Eye Res.* **209**,.

Varshney, G. K., Lu, J., Gildea, D. E., Huang, H., Pei, W., Yang, Z., Huang, S. C., Schoenfeld, D., Pho, N. H., Casero, D., et al. (2013). A large-scale zebrafish gene knockout resource for the genome-wide study of gene function. *Genome Res.* **23**, 727–735.

Vincent, P. F., Bouleau, Y., Petit, C. and Dulon, D. (2015). A synaptic F-actin network controls otoferlin-dependent exocytosis in auditory inner hair cells. *Elife* **4**, e10988.

Wan, J. and Goldman, D. (2016). Retina regeneration in zebrafish. *Curr. Opin. Genet. Dev.* **40**, 41–47.

Wasfy, M. M., Matsui, J. I., Miller, J., Dowling, J. E. and Perkins, B. D. (2014). Myosin 7aa-/- mutant zebrafish show mild photoreceptor degeneration and reduced electroretinographic responses. *Exp. Eye Res.* **122**, 65–76.

Williams, D. S., Aleman, T. S., Lillo, C., Lopes, V. S., Hughes, L. C., Stone, E. M. and Jacobson, S. G. (2009). Harmonin in the murine retina and the retinal phenotypes of Ushlc-mutant mice and human USH1C. *Investig. Ophthalmol. Vis. Sci.* **50**, 3881–3889.

Willoughby, J. J. and Jensen, A. M. (2012). Generation of a genetically encoded marker of rod photoreceptor outer segment growth and renewal. *Biol. Open* **1**, 30–36.

Yang, Z., Chen, Y., Lillo, C., Chien, J., Yu, Z., Michaelides, M., Klein, M., Howes, K. A., Li, Y., Kaminoh, Y., et al. (2008). Mutant prominin 1 found in patients with macular degeneration disrupts photoreceptor disk morphogenesis in mice. *J. Clin. Invest.* **118**, 2908–2916.

Zallocchi, M., Meehan, D. T., Delimont, D., Rutledge, J., Gratton, M. A., Flannery, J. and Cosgrove, D. (2012). Role for a novel Usher protein complex in hair cell synaptic maturation. *PLoS One* **7**, e30573.

Figures

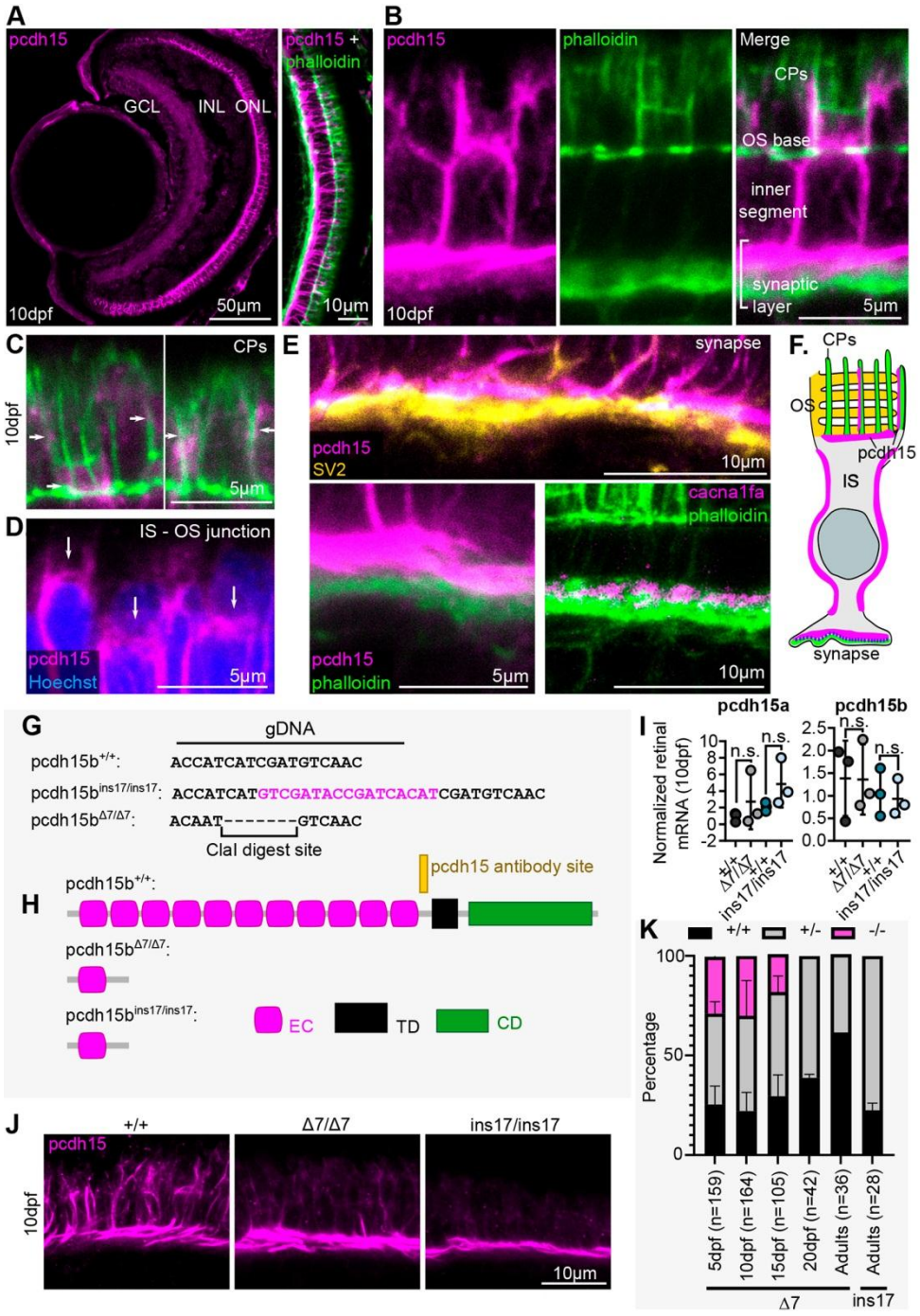

Figure 1. Pcdh15 is expressed in the photoreceptors of the zebrafish retina and is reduced in CRISPR generated pcdh15b mutants. (A) Representative images of the 10dpf retina stained with a pcdh15 antibody (magenta). Co-label with F-actin stain, phalloidin (green, present in the CPs and synapse) is shown for the central ONL. **(B)** Close up of a central region in the ONL stained with pcdh15 (magenta), phalloidin (green) and an overlap of the 2. **(C-D)** Close up of the co-staining of pcdh15 and phalloidin in the CPs **(C)** and of pcdh15 at the IS-OS junction **(D)**. **(E)** Representative images of SV2 staining (yellow), calcium channel 1.4_v staining (cacna1fa, magenta) in the photoreceptor synapse and its colocalization with pcdh15 and phalloidin (green) at 10dpf. **(F)** Schematic of pcdh15 expression in the zebrafish photoreceptor cell. Green= phalloidin in the synapse and CPs; magenta= pcdh15 in the CPs, OS base, IS membrane and synapse. Blue dots= calcium channel 1.4_v in the synapse. **(G)** gRNA used to target and mutate the pcdh15b gene. A 17bp insertion (*magenta bolded* nucleotides) and a 7bp deletion (*bolded black* nucleotides) mutant were identified. **(H)** Predicted results of the mutations on the protein sequence. EC= extracellular cadherin domains; TD= transmembrane domain; CD= variable cytoplasmic domain. **(I)** RT-qPCR to elevate the mRNA expression for pcdh15a and pcdh15b normalized to actin in wildtype siblings and pcdh15b mutants. **(J)** Pcdh15 staining in wildtype siblings +/+) and mutants (Δ7/Δ7 and ins17/ins17) at 10dpf (n=5+ for each genotype). GCL= ganglion cell layer, INL= inner nuclear layer, ONL= outer nuclear layer, CPs= calyceal processes, OS= outer segment, IS= inner segment. **(K)** Genotyping of clutches of heterozygous crosses up to adulthood to measure survival (number of fish genotyped (n) is indicated in the graph).

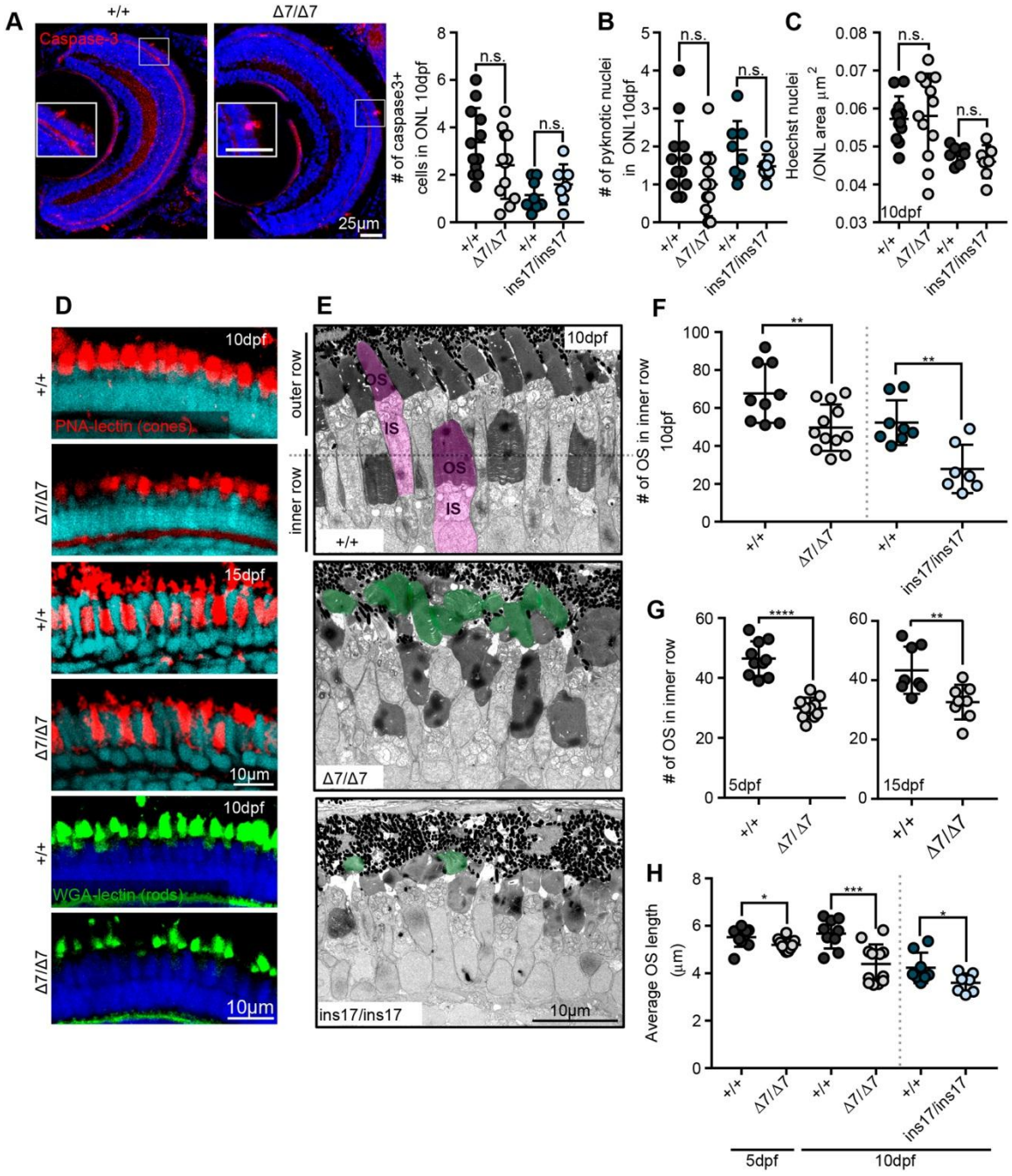

Figure 2. Cone and rod photoreceptors show a reduction in outer segment number and length, that is not attributed to cell death or loss. (A) Staining and quantification of cell death marker, cleaved (activated) caspase-3, at 10dpf in the ONL per section (+/+= 12 eyes) (Δ7= 12 eyes). **(B)** Quantification of the number of pyknotic nuclei in the ONL. **(C)** Photoreceptor nuclei

(Hoechst) density per micron area in the ONL at 10dpf measured from an average of 20µm thick sections. For **(B-C)**: +/+= 12 eyes; Δ7= 11 eyes, +/+= 8 eyes, ins17= 7 eyes. **(D-E)** Representative images of OS markers for cones (PNA lectin, red) and rods (WGA lectin, green) at 10dpf and 15dpf (D) and TEM images of the central retina of wildtype siblings (+/+) and Δ7 and ins17 mutants at 10dpf (E). Magenta= individual photoreceptor. Green= detached OS. OS= outer segment, IS= inner segment. **(F-G)** Quantification of the number of OS in the inner row at 10dpf (F), 5dpf and 15dpf (G). **(H)** Quantification of the average length of all outer segments in the retina per section in wildtype siblings and Δ7 and ins17 mutants at 5dpf and 10dpf. Statistical test in (A-C, F-H) were performed using student's t-tests. n.s.=not significant; *=p≤0.05, **=p≤0.01, ***p≤0.001. Number of eyes analyzed for TEM data in E-G: 5dpf: +/+= 10 eyes, Δ7/Δ7= 10 eyes; 10dpf: +/+= 9 eyes, Δ7/Δ7= 12 eyes; +/+= 8 eyes, ins17/ins17= 7 eyes; 15dpf: +/+= 8 eyes, Δ7/Δ7= 8 eyes. At least n=5 individuals were assessed for each immunostained marker.

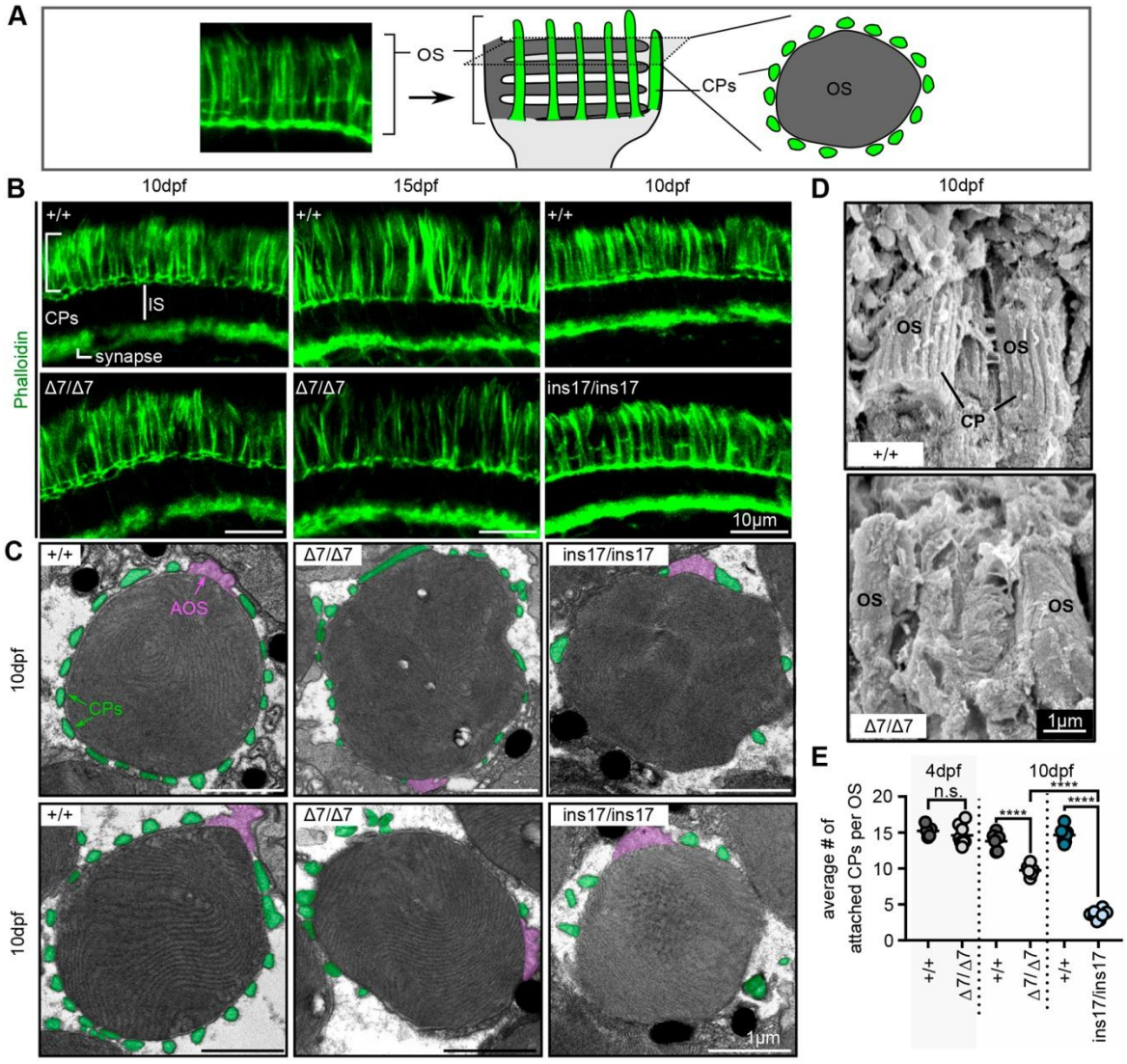

Figure 3. Calyceal processes are formed in pcdh15b mutants but are weakly attached and reduced/lost over time (A) Schematic illustrating CPs surrounding the OS of photoreceptors. The F-actin stain, phalloidin, is used to label CPs. Transverse sections along the length of the photoreceptor will show long CPs along their length, whereas horizontal cross-sections through the OS will show OS surrounded by a 'ring' of CPs. In all images CPs are coloured green. **(B)** Representative images of phalloidin staining in the photoreceptor layer in wildtype siblings (+/+) and Δ7 or ins17 mutants at 10dpf and 15dpf (n=8+ individuals for each genotype). **(C)**

Representative TEM images of horizontal cross-sections through the OS in wildtype siblings and Δ7 and ins17 mutants. CPs (connected or disconnected to the OS) are coloured green. AOS, accessory outer segments are coloured magenta. **(D)** Representative SEM images show CPs along the OS in wildtype siblings which is absent/decreased in Δ7 mutants. (n=5 eyes from 5 individuals per genotype). **(E)** Quantification of the average number of connected CPs per OS in wildtype siblings and pcdh15b mutants at 4dpf and 10dpf. OS quantified were sampled from the central retina in the ONL. Number of eyes analyzed for CP counts: 4dpf: +/+= 5 eyes, Δ7/Δ7= 8 eyes; 10dpf: +/+= 6 eyes, Δ7/Δ7= 6 eyes; +/+= 8 eyes, ins17/ins17= 8 eyes. Statistical test in (E) were performed using student's t-test for 4dpf and one-way ANOVA for 10dpf. n.s.=not significant; ****p≤0.0001. CPs= calyceal processes, IS= inner segment, OS= outer segment, AOS= accessory outer segment.

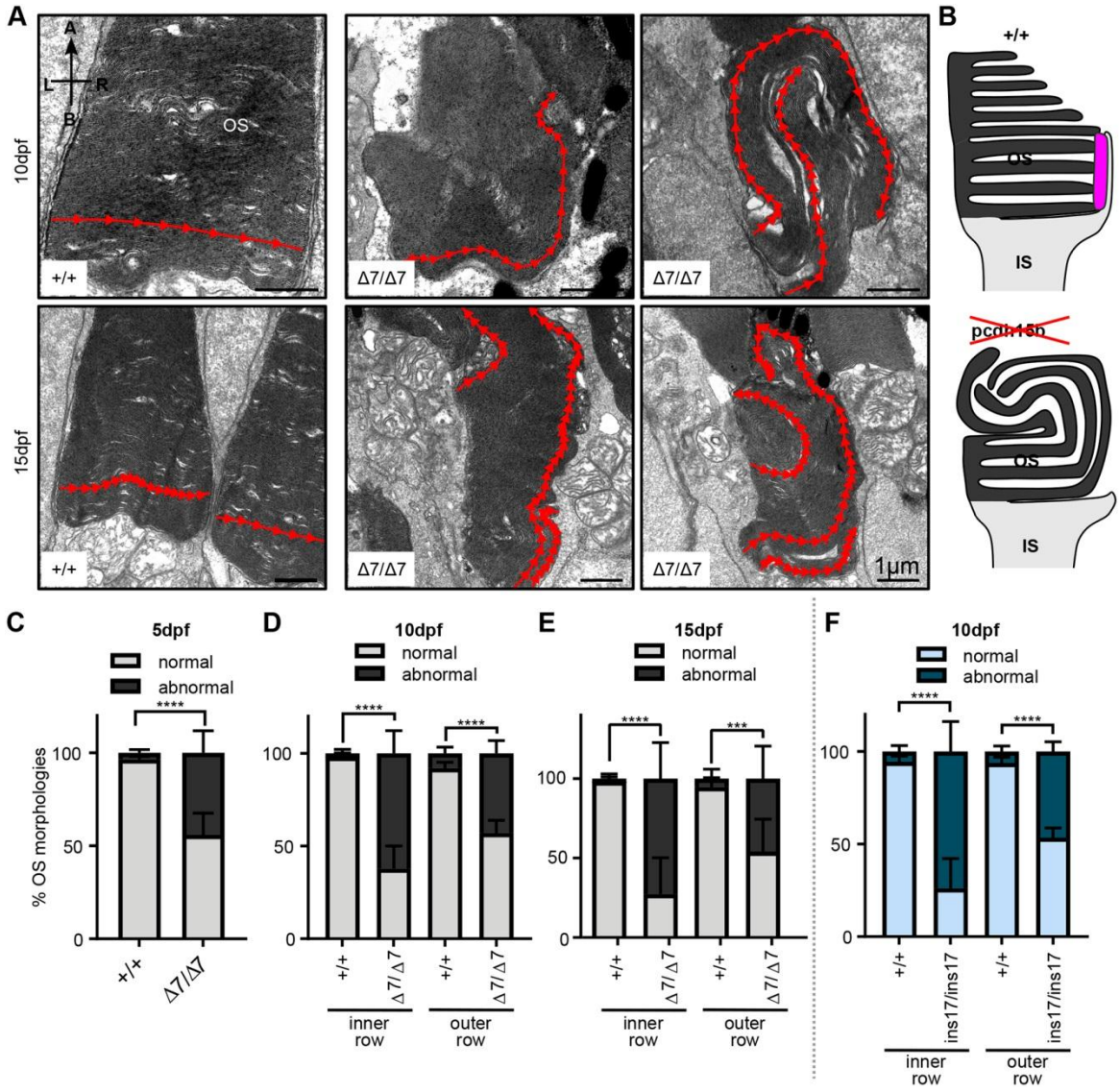

Figure 4. Ultrastructure of outer segments in pcdh15b mutant photoreceptors exhibit abnormal directional growth of outer segment discs. (A) Representative TEM images of OS of wildtype siblings and Δ7 mutants at 10dpf and 15dpf. Red arrow line shows disc direction. Directional arrows at the top left of the first image indicate positioning, A=apical, B=basal, L=left, R=right. **(B)** Schematic of the effects of pcdh15b mutation on the growth of the OS discs. Pcdh15 is shown in +/+ by magenta coloured shape. OS= outer segment, IS= inner segment. **(C-**

F) Quantification of the percentage of 'normal' and abnormal OS in wildtype siblings and pcdh15b mutants at different time points and mutant types (Δ7 and ins17). Statistical tests in (C-F) were performed using student t-tests. ***=p≤0.001, ****=p≤0.0001. OS were analyzed across the entire ONL for the 5 and 10dpf data, and the central retina for 15dpf data. Number of eyes analyzed: (B) 5dpf: +/+= 10 eyes, 2123 OS analyzed; Δ7/Δ7= 10 eyes, 1874 OS analyzed; (C) 10dpf: +/+= 9 eyes, 1990 OS analyzed; Δ7/Δ7= 12 eyes, 2457 OS analyzed; (D) 15dpf: +/+= 6 eyes, 320 OS analyzed; Δ7/Δ7= 6 eyes, 291 OS analyzed; (E) 10dpf: +/+= 8 eyes, 1260 OS analyzed; ins17/ins17= 7 eyes, n= 956 OS analyzed.

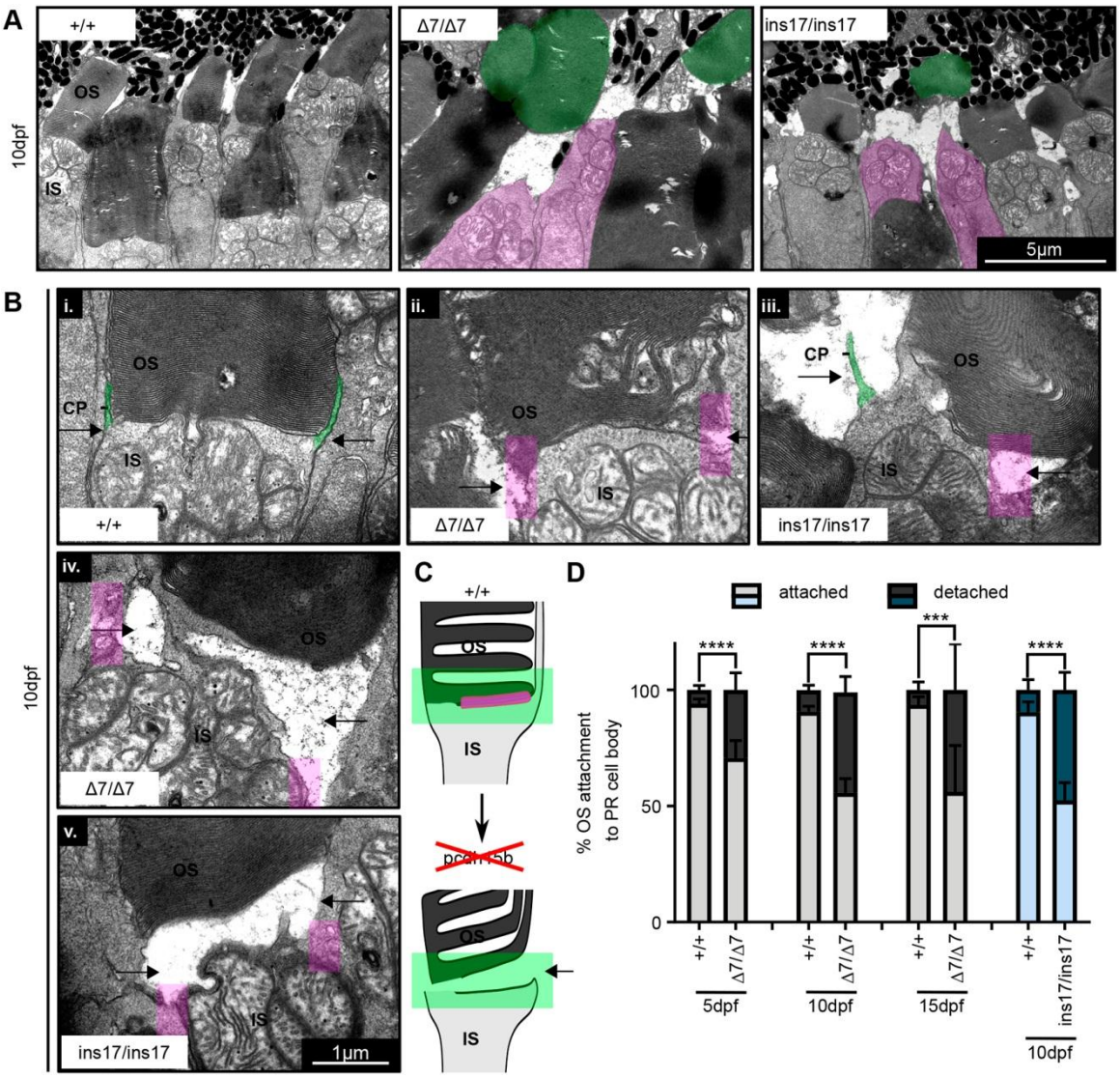

Figure 5. Outer segment detachment from the photoreceptor cell body is increased in pcdh15b mutants. (A) Representative TEM images of OS detachment and floating OS seen in pcdh15b mutants (Δ7 and ins17), compared to wildtype siblings. Magenta is used for IS with no OS and green is used for detached 'floating' OS. These phenomena are rarely observed in wildtype siblings. **(B)** Close-up TEM examples of OS to IS connection in photoreceptors of wildtype siblings and Δ7 and ins17 mutants showing the process of detachment. CPs are visible

as protrusions coming up from the IS (*green* coloured) and attaching to the sides of the OS (*arrows point to the sides*). Pcdh15b mutants (Δ7/Δ7 and ins17/ins17) show a range of affected connections (i-v), coincident with the lost of CP (*magenta* coloured box) attachments on the sides (*arrows*). **(C)** Schematic of the OS detachment seen in pcdh15b mutants. The relevant pcdh15 expression at the OS base is highlighted in magenta. The green box highlights the IS-OS connection. (**D)** Quantification of the percent of total identified photoreceptor IS/cell bodies with attached or completely detached/missing OS across the entire ONL from 5-15dpf. Statistical tests were performed using student's t-test. ***=p≤0.001, ****=p≤0.0001. Number analyzed: 5dpf: +/+= 10 eyes, 1780 PR; Δ7/Δ7= 10 eyes, 1473 PR; 10dpf: +/+= 9 eyes, 1844 PR; Δ7/Δ7= 12 eyes, 2290 PR; 15dpf: +/+= 6 eyes, 334 PR; Δ7/Δ7= 6 eyes, 474 PR; 10dpf: +/+= 8 eyes, 1253; ins17/ins17= 7 eyes, n= 1087 PR (PR=photoreceptor). ONL= outer nuclear layer, CPs= calyceal processes, OS= outer segment, IS= inner segment.

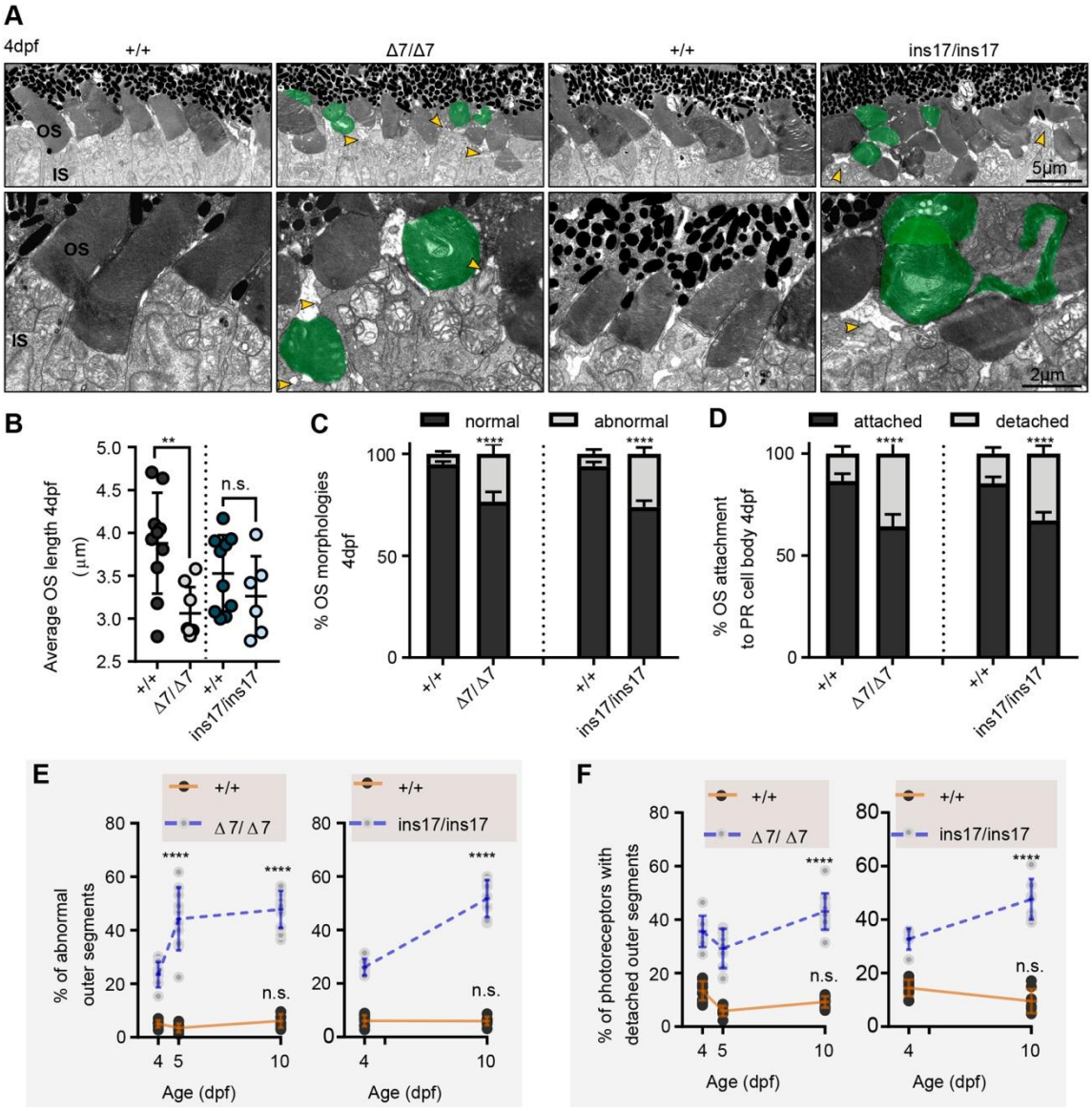

Figure 6. Photoreceptors in pcdh15b mutants develop with defects and get progressively worse with age. **(A)** Representative TEM images of the central ONL (top) and OS (bottom) in wildtype siblings, Δ7 and ins17 mutants at 4dpf. Green= deformed/abnormal OS. Yellow arrowheads point to regions of disconnection between the IS and OS. **(B-D)** Quantification of the average length of all outer segments in the retina per section **(B)**, the proportion of OS morphologies **(C)** and the percent of attached/detached OS **(D)** in wildtype siblings, Δ7 and

ins17 mutants at 4dpf. The entire ONL was used for quantification. **(E-F)** Developmental trend of the percentage of abnormal OS **(E)** and photoreceptors with detached outer segments **(F)** in the retina from 4-10dpf in wildtype siblings, Δ7 or ins17 mutants. Statistical tests were performed using t-tests (B, C, D) and 2-way ANOVA (E, F). n.s.=not significant; **=p≤0.01, ****=p≤0.0001. Number analyzed: +/+= 10 eyes and 1528 OS analyzed, Δ7/Δ7= 8 eyes and 1412 OS analyzed; +/+= 10 eyes and 1829 OS analyzed, ins17/ins17= 6 eyes and 1328 OS analyzed. ONL= outer nuclear layer, OS= outer segment, IS= inner segment.

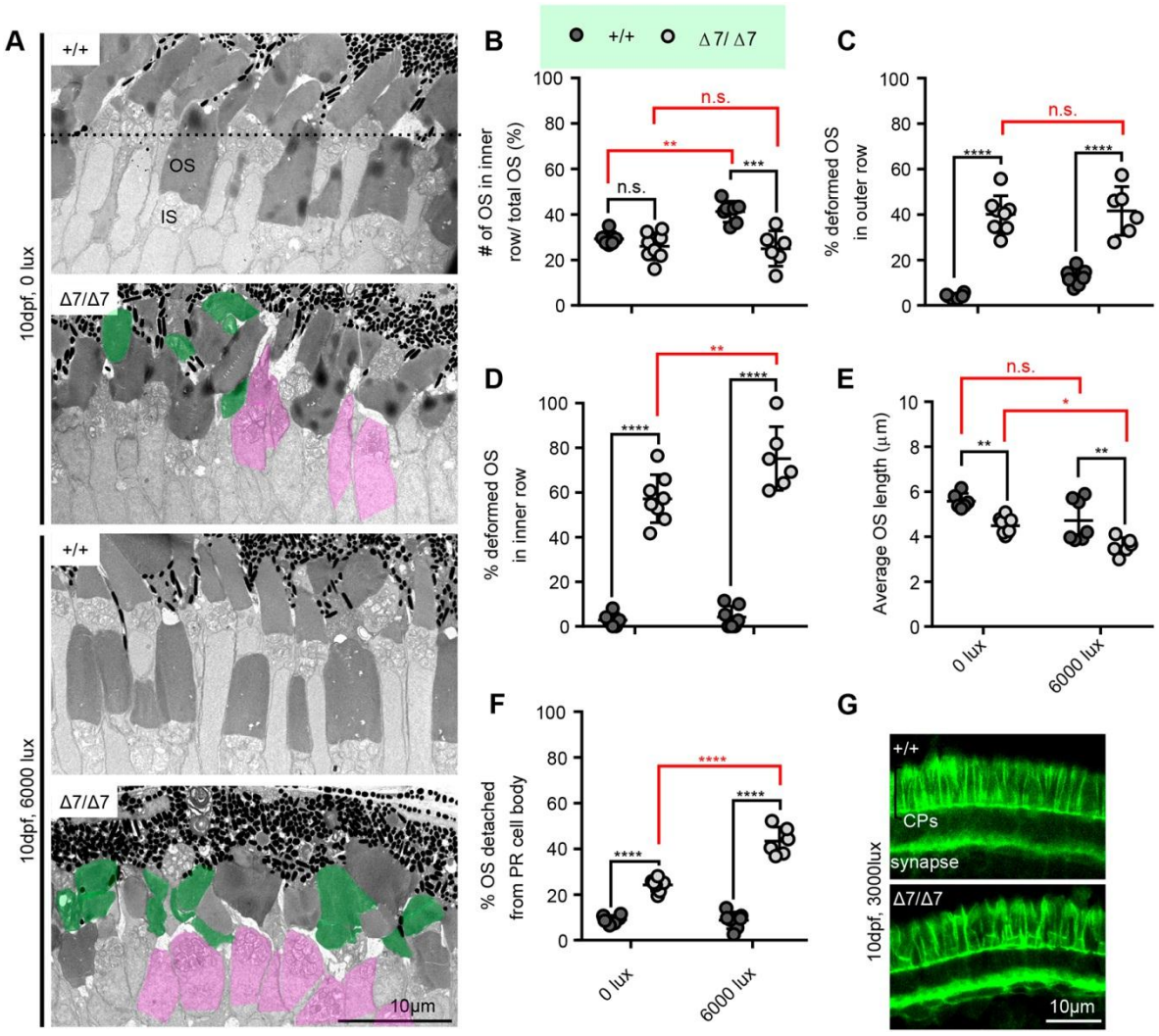

Figure 7. Differential light exposure in pcdh15b mutants attenuates or exacerbates photoreceptor defects. (A) Representative TEM images of wildtype sibling and pcdh15b mutant ONL at 10dpf grown under 0 lux (dark) and 6000 lux (bright) light conditions. The line in the top image separates the inner and outer row. IS with detached OS are coloured magenta. Deformed OS are coloured green. **(B-F)** Quantification of the percent of total OS found in the inner row (B), the percent of deformed outer segments in the outer row (C) and the inner row (D), average OS length (E), and percent of total identified photoreceptor IS/cell bodies with attached or

completely detached/missing outer segment (F) across the retina photoreceptor layer under different light conditions in wildtype siblings and pcdh15 Δ7 mutants. All graphs from B-F use the same labelling in (B) to distinguish between +/+ and Δ7/Δ7. X-axis labels are the same and seen at the bottom in (E) and (F). **(G)** Representative phalloidin staining in the ONL, labelling CPs, at 10dpf when exposed to 3000 lux bright light (+/+ n=7 eyes, Δ7/Δ7 n=7 eyes). 0 lux measurements were taken across the entire ONL, and 6000 lux measurements were taken only in the central ONL. Statistical tests in (B-D, F) were performed using two-way ANOVA. Statistical tests in E were performed using one-way ANOVA. n.s.= not significant, *=p≤0.05, **=p≤0.01, ***=p≤0.001, ****=p≤0.0001. Numbers analyzed: 0 lux: +/+= 6 eyes, 1239 OS analyzed; Δ7/Δ7= 8 eyes, 1623 OS analyzed; 6000 lux: +/+= 7 eyes, 541 OS analyzed; Δ7/Δ7= 6 eyes, 409 OS analyzed. OS= outer segment, IS= inner segment.

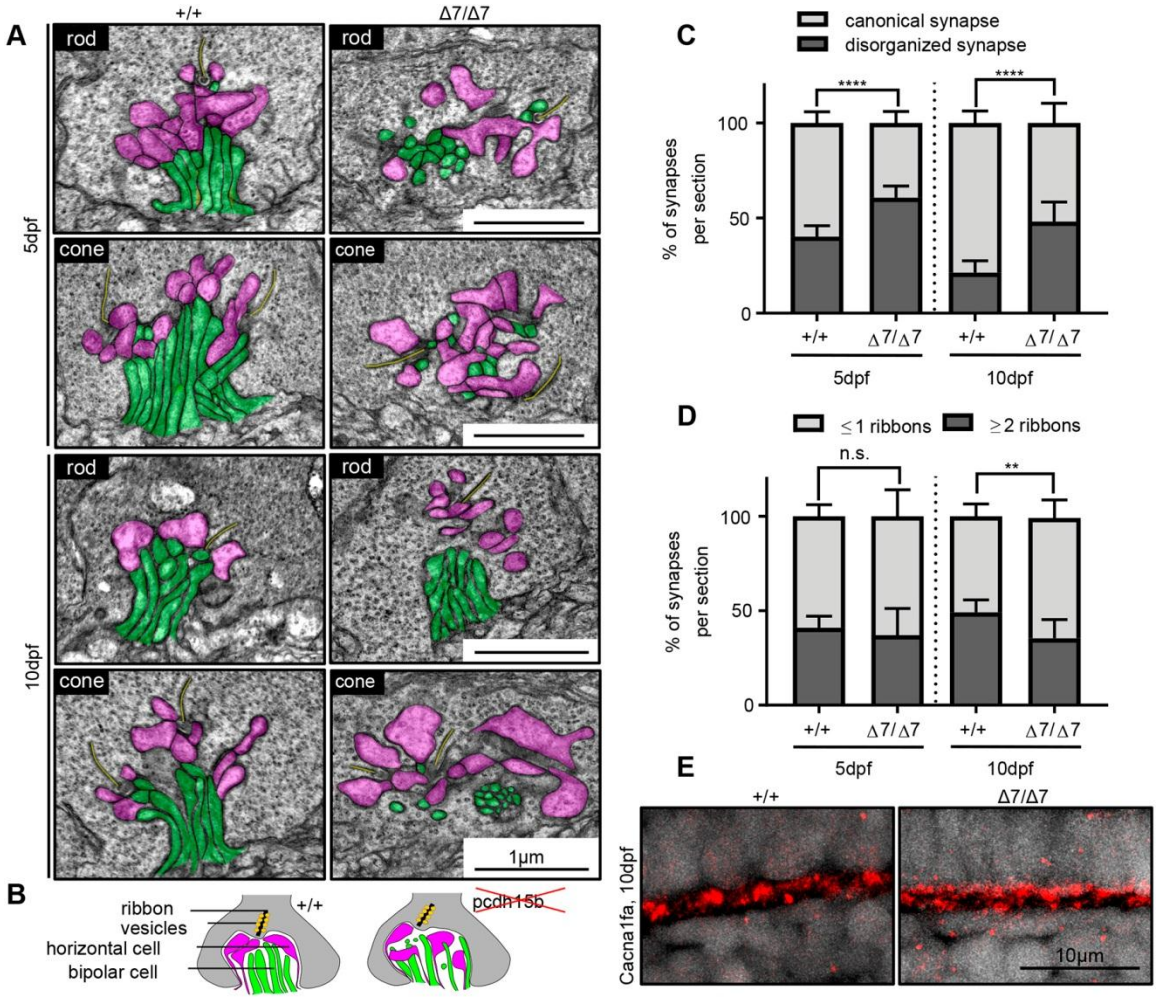

Figure 8. Photoreceptor ribbon synapses show increased disorganization in pcdh15b mutants.

(A) Representative TEM images of photoreceptor ribbon synapses from both rod and cone terminals in wildtype siblings and pcdh15b Δ7 mutants at 5 and 10dpf. Bipolar cell innervations (*green*), and horizontal cell innervations (*pink*) into photoreceptor termini and ribbon synapses (*yellow*) are highlighted. **(B)** Schematic of synaptic structure in wildtype and pcdh15b mutants. Magenta= horizontal cell processes, green= bipolar cell processes. Ribbons are shown as a black line, surrounded by yellow-coloured vesicles. **(C)** Quantification of the percent of synapses that display a canonical or disorganized synapse organization in wildtype siblings and Δ7 mutants at

5 and 10dpf. **(D)** Quantification of the percent of synapses that contain one or less ribbons (usually associated with rod termini), or two or more ribbons (usually associated with cone termini) in wildtype siblings and Δ7 mutants at 5 and 10dpf. **(E)** Representative images of calcium channel 1.4_v staining (cacna1fa) in the outer plexiform layer, at photoreceptor termini (n=5+ individuals for each genotype). Statistical tests in (C and D) were performed using students t-tests. n.s.= not significant; **= p≤ 0.01, ****= p≤ 0.0001. Number analyzed: 5dpf: +/+= 10 eyes, 620 synapses analyzed; Δ7/Δ7= 10 eyes, 593 OS analyzed; 10 dpf: +/+= 8 eyes, 201 synapses analyzed; Δ7/Δ7= 8 eyes, 192 synapses analyzed. Synapses used in quantification were samples from the central ONL.

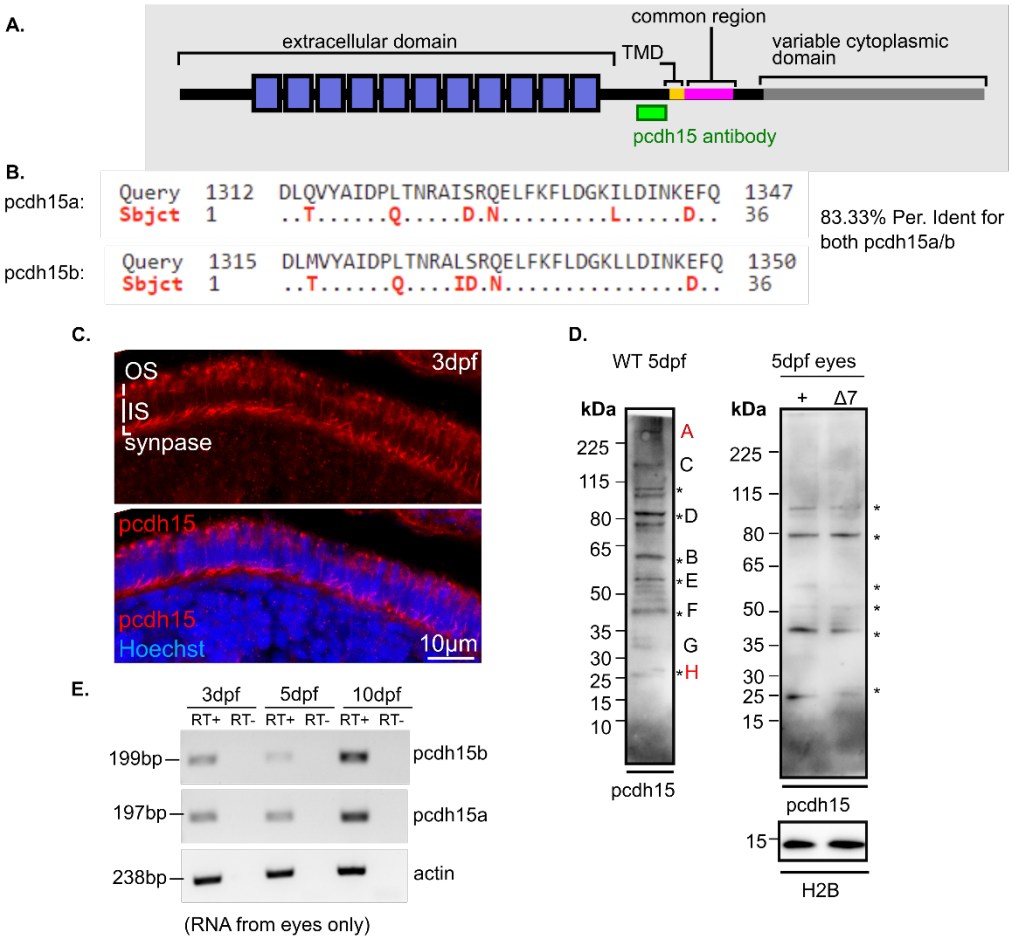

Fig. S1. Generation of pcdh15b mutants by CRISPR. (A) Schematic of pcdh15 protein and the relevant domains (TMD= transmembrane domain) and the locations of the pcdh15 antibody. (B) Alignment of the antigen recognized by the pcdh15 antibody and pcdh15a (top) and pcdh15b (bottom). Query= pcdh15a/b protein sequence; Sbjct (red)= Mismatches from the antibody antigen sequence. **(C)** Representative image of pcdh15 expression in the 3dpf retina at the ONL. OS= outer segment, IS= inner segment, ONL= outer nuclear layer, INL= inner nuclear layer. **(D)** Western blot analysis of the pcdh15 antibody in isolated WT and mutant retinas. The * bands are the well-defined bands in each blot. The lettering (A-H) correspond to bands previously seen and described in (Alagramam et al., 2011). **(E)** RT-PCR of *pcdh15a*, *pcdh15b* and control actin mRNA in 3dpf, 5dpf and 10dpf eyes. **(F, H)** Representative sequencing chromatograms of wildtype siblings (left panels) and mutants (Δ7 (F), ins17 (H)) (right panels), with highlighted bands showing the affected regions (*grey* for 7bp deletion and *red* for 17bp insertion). **(G)** In addition to sequencing, the 7bp deletion (but not the 17bp insertion) can be identified by the loss of a ClaI digest site resulting in an uncut large band, as shown in the representative gel.

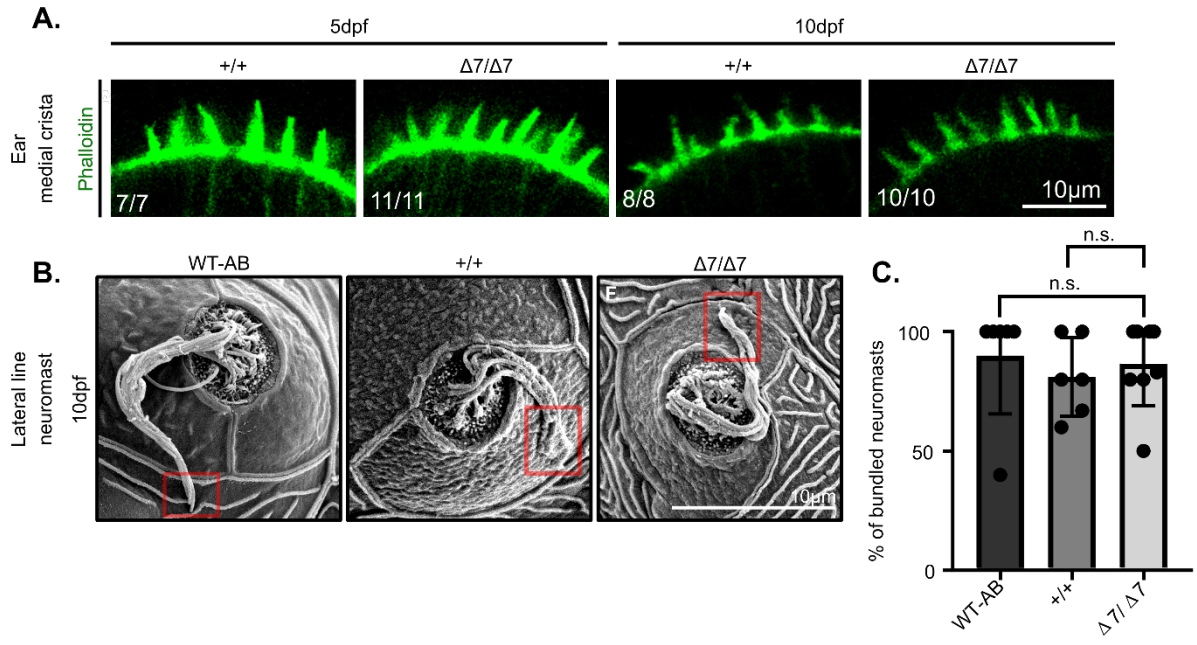

Fig. S2. Hairs cells of the inner ear and lateral line are unaffected in pcdh15b mutants. (A) Representative images of stereocilia, found in hair cells of the medial crista of the inner ear, labelled by phalloidin (*green*) in wildtype siblings (+/+) and pcdh15b mutants (Δ7/Δ7) at 5dpf (n=7, 11) and 10dpf (n= 8, 10). **(B)** Representative SEM images of neuromasts along the lateral line in unrelated wildtype-AB (WT-AB), wildtype siblings (+/+) and pcdh15b mutants (Δ7/Δ7). Red boxes highlight the bundled tips found in each neuromast. **(C)** Quantification of bundled neuromast tips. One-way ANOVA n.s.= p>0.05. Each individual graph point represents the percent of bundled tips from an average of at least 5 neuromasts examined per individual (WT-AB n=6, +/+ n=6, Δ7/Δ7 n=8).

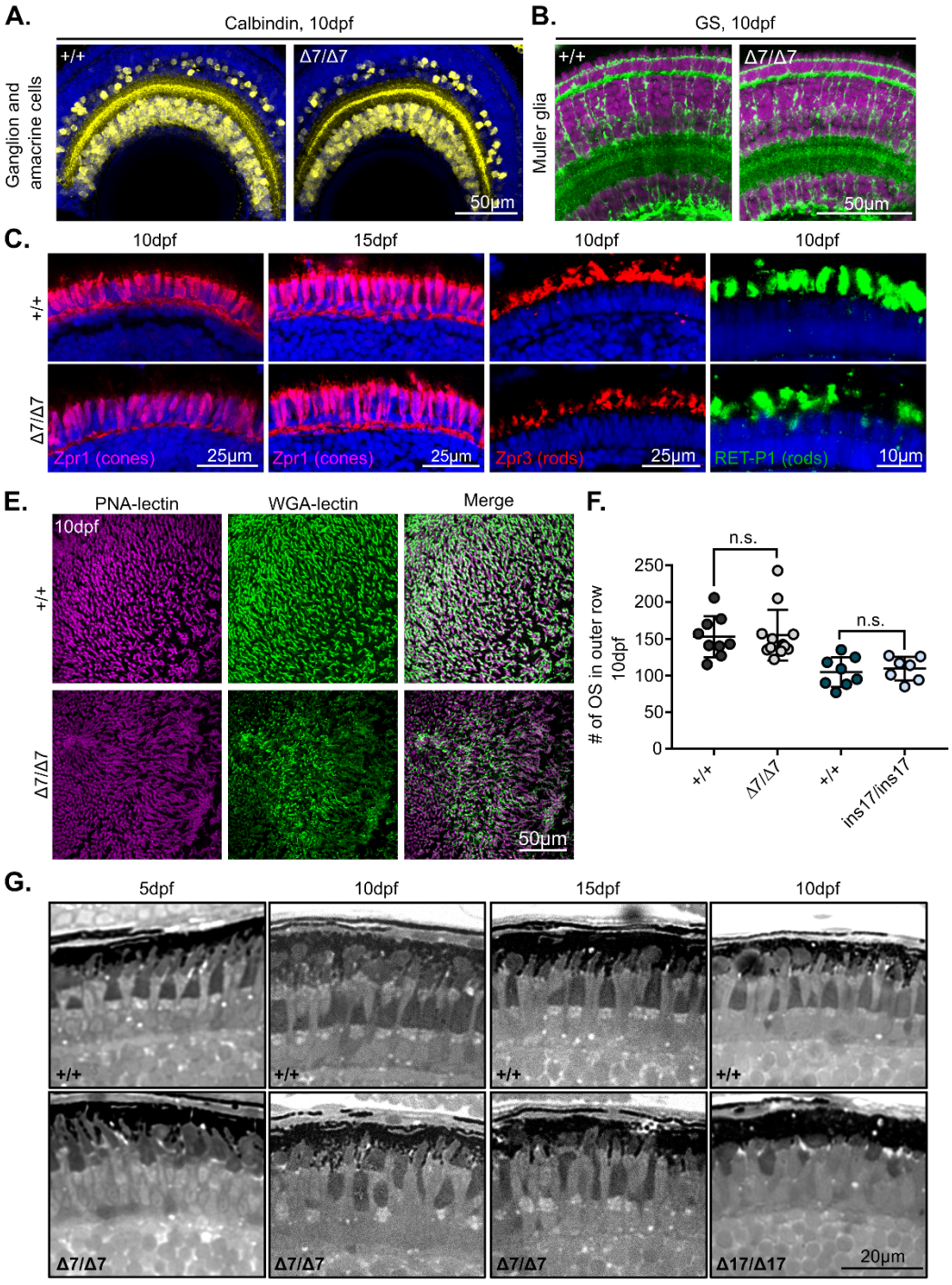

Fig. S3. Abnormalities in the pcdh15 mutant retina is restricted to the cone and rod photoreceptors. (A) Representative images of calbindin (*yellow*), a ganglion and amacrine cell marker, and **(B)** glutamine synthetase (GS) (*green*), a Muller glia cell marker, at 10dpf in wildtype sibling and Δ7

mutant retinas. Nuclei are counterstained with Hoechst (*Blue (A) /magenta (B)*). **(C)** Representative images from different cone and rod photoreceptor markers in wildtype siblings and Δ7 mutants at 10dpf and 15dpf. Zpr1 labels red-green double cone cell bodies (*magenta*). Zpr3 labels a rod outer segment component (*red*). RET-P1, labels rhodopsin in outer segments (*green*). Nuclei are counterstained with Hoechst (*blue*). **(E)** Whole mount immunostaining of the retina, in wildtype siblings (n=17) and Δ7 mutants (n=10) by WGA-lectin (*green*), and PNA-lectin (*magenta*) at 10dpf. **(F)** The number of OS found in the 'outer row' of the photoreceptor layer of wildtype siblings and pcdh15b mutants at 10dpf measured in TEM images across the entire ONL. **(G)** Representative semi-thin sections of the photoreceptor layer of pcdh15b mutants (Δ7, ins17) and their wildtype siblings from 5-15dpf.

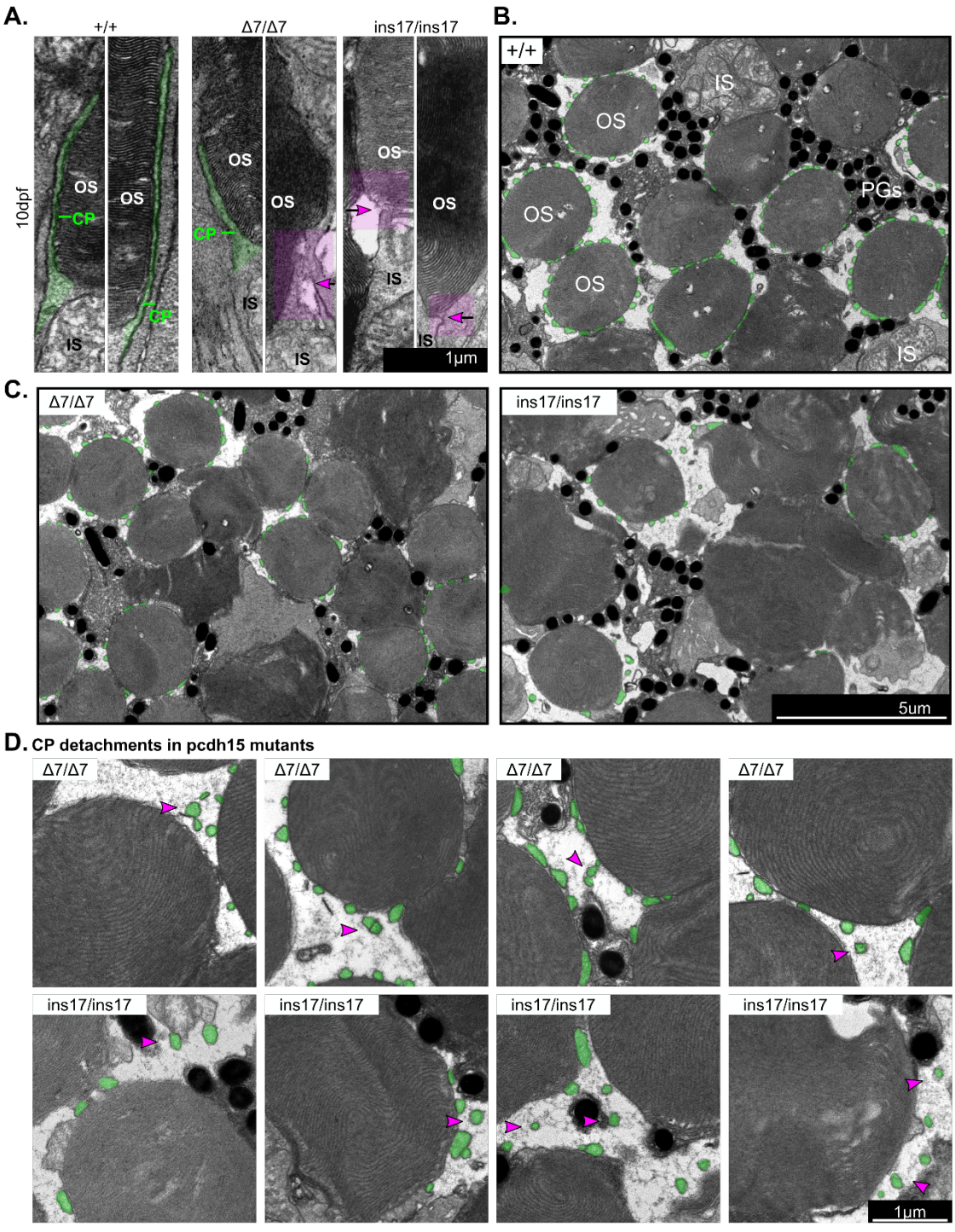

Fig. S4. CPs become detached and are eventually lost/reduced in pcdh15b mutant photoreceptors. (A) Representative TEM images of CPs found on the side of OS in wildtype sibling and pcdh15b mutant photoreceptors. CPs are highlighted in green. Regions in pcdh15b

mutants that have lost CPs are highlighted in magenta and shown with a magenta arrow. **(B-C)** Overview representative images of horizontal TEM sections through the photoreceptor layer in wildtype siblings (B) and mutants (C). CPs surrounding photoreceptor OS are coloured green. Abnormal OS shape in mutants can also be seen in these sections. **(D)** Multiple examples from horizontal TEM sections showing CP detachment (magenta arrowhead) in the different pcdh15b mutants (Δ7 and ins17). All visible CPs are coloured green. CPs= calyceal processes, OS= outer segment, IS= inner segment, PGs= pigment granules.

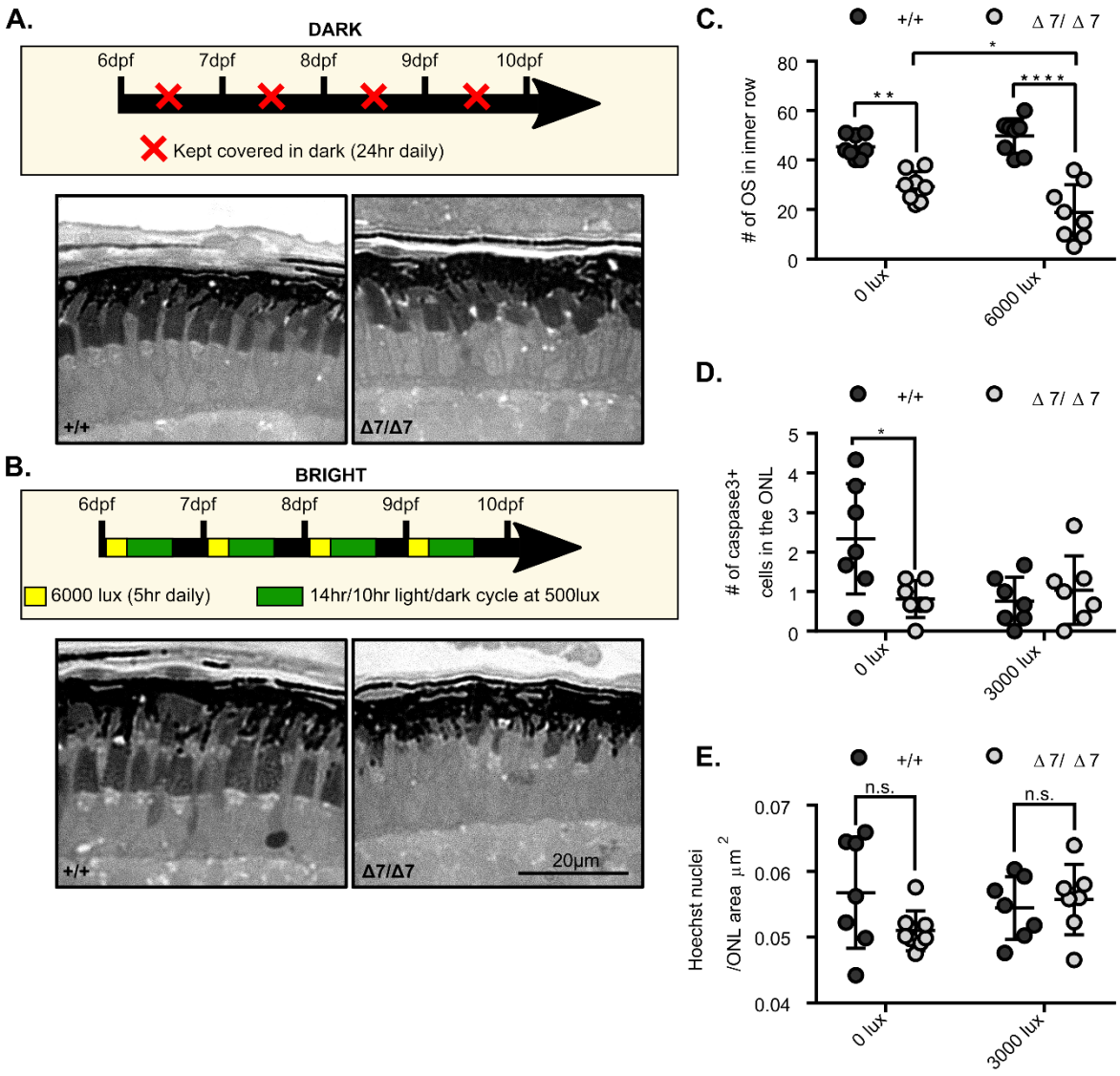

Fig. S5. Light exposure influences the severity of abnormalities in the photoreceptors of pcdh15b mutants. (A-B) Wildtype siblings and Δ7 mutants were grown under dark conditions (0 lux) (A) or bright light conditions (6000 lux) (B) from 6-10dpf. Representative semi-thin retinal sections (1μm thick) of wildtype sibling (n=8 eyes (0 lux), 8 eyes (6000 lux)) and Δ7 mutants (n=8 eyes (0 lux), 8 eyes (6000 lux)) under each condition at 10dpf. **(C)** Quantification of the number of OS in the inner row across a semi-thin section in the different light conditions. **(D-E)** Quantification of the number of caspase-3+ cells in the ONL/section (D) and photoreceptor

density (Hoechst nuclei/ONL area) between wildtype siblings (n=7 eyes (0 lux), 7 eyes (3000 lux)) and Δ7 mutants (n=7 eyes (0 lux), 7 eyes (3000 lux)) (E) under the different light conditions. Statistical tests in (C, D, E) were performed using two-way ANOVA. *=p≤0.05, **=p≤0.01, ****=p≤0.0001.

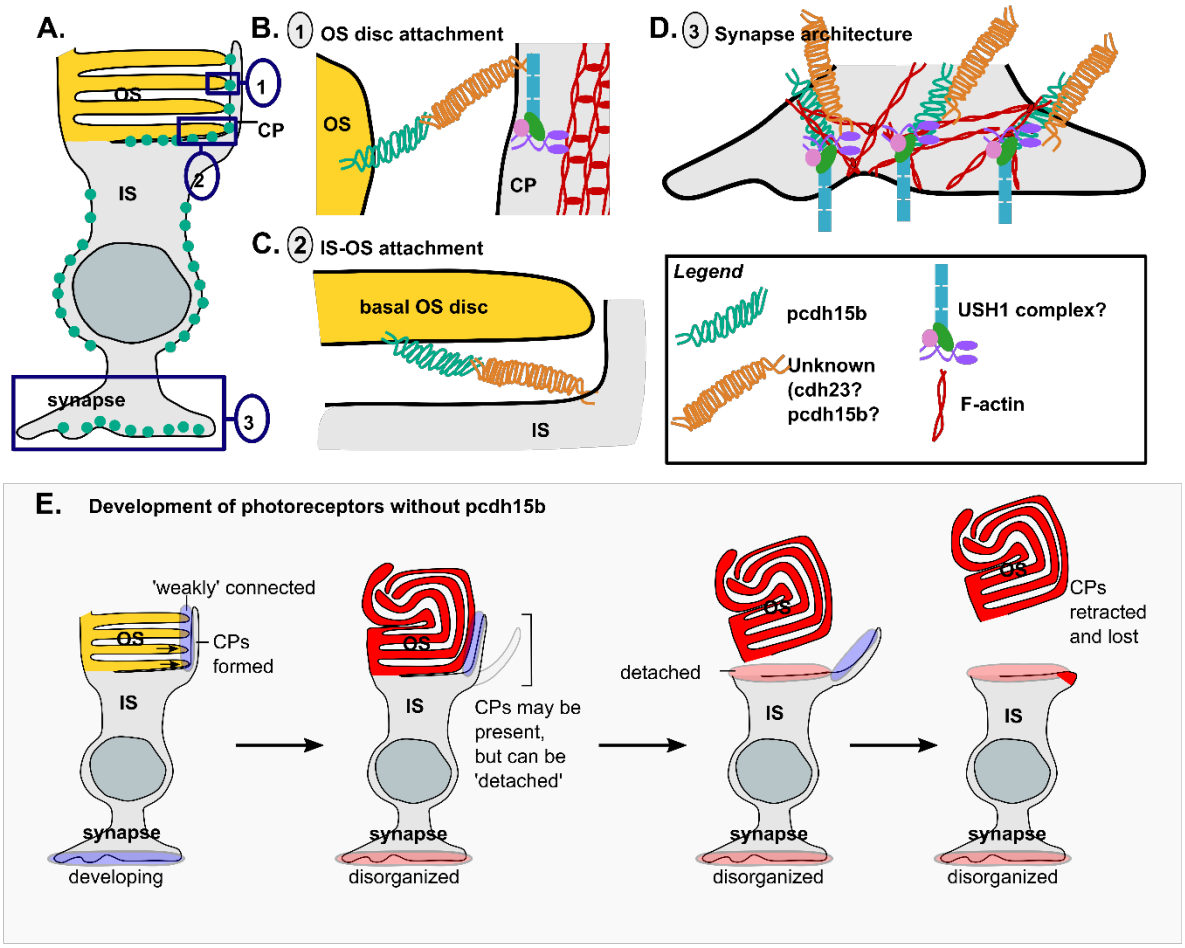

Fig. S6. Model of pcdh15b function in the zebrafish retina. These data suggest that zebrafish pcdh15b functions at 3 main subcellular compartments in the photoreceptor: the CPs, the IS-OS junction and the synapse. **(A)** Schematic of the photoreceptor and location of pcdh15b expression based on our pcdh15 expression data. OS= outer segment, IS= inner segment, CP= calyceal processes. Green dots are locations of pcdh15 expression. Blue boxes are the regions examined more closely in (B-D). **(B)** Close up OS disc schematic of the attachment between OS discs and the CP mediated by pcdh15, and possible other proteins not yet clarified in zebrafish. **(C)** Close up of the IS-OS attachment between the basal OS disc and the IS plasma membrane by pcdh15 **(D)** Close up schematic of how pcdh15 (and other USH1 proteins) organized the actin

cytoskeleton and synapse in photoreceptors. (E) Schematic of the photoreceptor developing in the absence of pcdh15b. Images left to right: (First) As the photoreceptor develops the discs of the OS start to move towards a formed CP protrusion, however it does not form a strong attachment. (2) Without a strong attachment, the OS discs instead continue to grow in abnormal directions. By the time the synapses mature, they are disorganized. (3) The OS will eventually detach as pcdh15 is not there to secure the attachment to the IS plasma membrane. CPs will start to fall away. (4) The detached OS will float further away from the rest of the photoreceptor and eventually the CP will be completely lost and retracted. Retraction may occur earlier in the previous stages. Red colouring in the image highlights regions that have become defective in the photoreceptor.